DENTAL MATERIALS 35 (2019) 368–388

Available online at www.sciencedirect.com

ScienceDirect

journal homepage: www.intl.elsevierhealth.com/journals/dema

Translational research on clinically failed zirconia implants

Susanne S. Scherrer[a,*], *Mustapha Mekki*[a], *Claude Crottaz*[b], *Michael Gahlert*[c,d], *Eric Romelli*[e], *Laurine Marger*[a], *Stéphane Durual*[a], *Eric Vittecoq*[f]

[a] *Division of Fixed Prosthodontics and Biomaterials, University Clinic of Dental Medicine, University of Geneva, Geneva, Switzerland*

[b] *Unit of Oral Surgery and Implantology, Department of Surgery, University Hospitals of Geneva, Geneva, Switzerland*

[c] *Clinic for Oral and Cranio-Maxillofacial Surgery, Hightech Research Center, Basel, Switzerland*

[d] *Private Dental Clinic, Munich, Germany*

[e] *Division of Cariology and Endodontology, University Clinic of Dental Medicine, University of Geneva, Geneva, Switzerland*

[f] *HEPIA, University of Applied Sciences – Western Switzerland (HES-SO), Geneva, Switzerland*

ARTICLE INFO

Article history:
Received 26 July 2018
Received in revised form
27 November 2018
Accepted 28 November 2018

Keywords:
Fracture
Zirconia
Implants
Fractography
Bending moment
Clinical failure

ABSTRACT

Objectives. To provide fractographic analysis of clinically fractured zirconia implants recovered with their cemented crown. To calculate bending moments, corresponding stress and crack onset location on the implant's fracture surface using a mathematical model integrating spatial coordinates of the crown-implant part and occlusal loading obtained from 2D and 3D images.

Methods. 15 fractured zirconia implants parts (11 posterior and 4 anterior) with their all-ceramic crowns still cemented on it were recovered. The implants were first generations from four manufacturers (AXIS Biodental, Z-Systems, Straumann, Swiss Dental Solutions). The time-to-failure varied between 2 weeks and 9 years. Fractography was performed identifying the failure origin and characteristic surface crack features. From 2D and 3D digital images of the crown-implant part, spatial coordinates anchoring the crown's occlusal contacts with the implant's central axis and reference plane were integrated in a mathematical model spreadsheet. Loads of 500 N in total were selectively distributed over identified occlusal contacts from wear patterns. The resultant bending and torsion moments, corresponding shear, tensile, maximum principal stress and von Mises stress were calculated. The fracture crack onset location on the implant's fracture surface was given by an angular position with respect to an occlusal reference and compared with the location of the fracture origin identified from fractographic analysis.

* *Corresponding author at*: Division of Fixed Prosthodontics and Biomaterials, University Clinic of Dental Medicine, University of Geneva, 1, rue Michel-Servet, 1204 Geneva, Switzerland.

E-mail addresses: susanne.scherrer@unige.ch (S.S. Scherrer), mustapha.mekki@unige.ch (M. Mekki), claude.crottaz@hcuge.ch (C. Crottaz), info@drgahlert.com (M. Gahlert), eric.romelli@unige.ch (E. Romelli), laurine.marger@unige.ch (L. Marger), stephane.durual@unige.ch (S. Durual), eric.vittecoq@hesge.ch (E. Vittecoq).

https://doi.org/10.1016/j.dental.2018.11.033

Results. Implants fractured from the periphery of the smaller inner diameter between two threads at the bone-entrance level except for one implant which failed half-way within the bone. The porous coating (AXIS Biodental) and the large grit alumina sandblasting (Z-System) created surface defects directly related to the fracture origin. The model spreadsheet showed how occlusal loading with respect to the implant's central axis affects bending moments and crack onset. Dominant loads distributed on contacts with important wear pattern provided a calculated crack onset location in good agreement with the fractographic findings of the fracture origin.

Significance. Recovered broken zirconia implant parts with their restorative crowns can provide not only information regarding the failure origin using fractography but also knowledge regarding occlusal crown loading with respect to the implant's axis. The mathematical model was helpful in showing how occlusal loading affects the location of the fracture initiation site on clinical zirconia implant fracture cases.

1. Introduction

Translational research is performed at the interface of basic and clinical sciences usually during short preclinical trials prior to launch on the market a new medical device or biomaterial. Translational research is there to catch any adverse effects seen during such preclinical trials and to make the needed modifications to improve the material for better long-term results. But translational research can also be applied throughout the lifetime of a product as knowledge can be gained from understanding the material's behavior under intraoral function especially when failed parts can be recovered for transdisciplinary material science investigation. Premature fracture of a brittle biomaterial under function such as that of a zirconia dental implant should be investigated using a multidisciplinary approach, combining knowledge from material sciences, fracture mechanics and clinical-related variables to better understand the reasons for failure [1]. A thorough microscopic analysis of the broken part can often provide key information as to the fracture origin and associated flaws, respectively unfavorable surface treatment, implant design issues or critical patient-specific loading conditions. Fractography is a powerful tool for microscope-based fracture surface analysis and is associated with fracture mechanics principles developed for brittle structures such as ceramics [2,3]. It has been successfully used in the dental field for understanding clinical fractures of ceramic fixed prosthetic restorations [3–7]. A guidance paper to the use of fractography in failure analysis of brittle materials has recently been published [5].

Zirconia implants have been brought to the dental market as a viable alternative to titanium implants initially to fulfill a demand from patients for non-metallic materials [8]. Thanks to its high biocompatibility, mechanical properties and interesting transformation toughening mechanisms under the application of a stress, zirconia is currently the structural ceramic used for dental biomedical applications [9–12]. Optimum performance of this biomaterial is however very dependent on the processing selected by the manufacturer and powder composition. The compaction, shape forming, sintering conditions, final grain size, amount of tetragonal and cubic phases are all processing related steps that will determine the material's mechanical properties and susceptibility to low temperature degradation (LTD) which remains a concern for the material's long-term stability [9,13–17]. On the esthetic level, zirconia is superior to titanium as no dark discoloration may appear through a thin soft peri-implant tissue [18]. On the biological side, zirconia is inert and therefore highly biocompatible. No corrosion products are formed in the oral cavity by zirconia implants as opposed to titanium implants, but the soft tissue response as well the bone-implant contact are similar providing some micro-rough surface is present [19]. On the mechanical side however, titanium has a 20–30 times higher fracture toughness for grade 4 titanium (K_{Ic} = 90–140 MPa$\sqrt{m}$) than 3Y-TZP (K_{Ic} = 4–7 MPa$\sqrt{m}$). In addition, titanium has an elongation of approximately 15% at break values allowing for some ductility which is negligible for zirconia.

When it comes to critically assess if zirconia is a viable alternative to titanium, the current review publications conclude that more high-evidence level clinical studies are needed, including more long-term RCT's to confirm current favorable outcomes of zirconia implants [19–24]. To better understand this statement, one has to consult the most recent systematic reviews for zirconia implants which reported survival rates of 92% [20] and 95.6% [23] after one year with an expected decrease of 0.25% after 5 years [23] based on prospective clinical trial information. The reported failures were primarily non-integration or loss of integration after some time of loading or after immediate loading. Although zirconia is less tough than titanium, the fracture of zirconia implants seems to be a rare event and has been documented using fractography in only two clinical trials [25,26]. Even if fracture of implants is rare, a thorough investigation of each failure case is worth the effort as it may provide useful information regarding issues related to implant design, diameter and surface treatment. Among the most probable causes cited for zirconia implant fracture are unfavorable narrow diameters, damaging surface treatments resulting from aggressive alumina sandblasting, and patient-related overloading [25,27]. If surface flaws resulting from processing problems involved in the crack initiation process can be determined using frac-

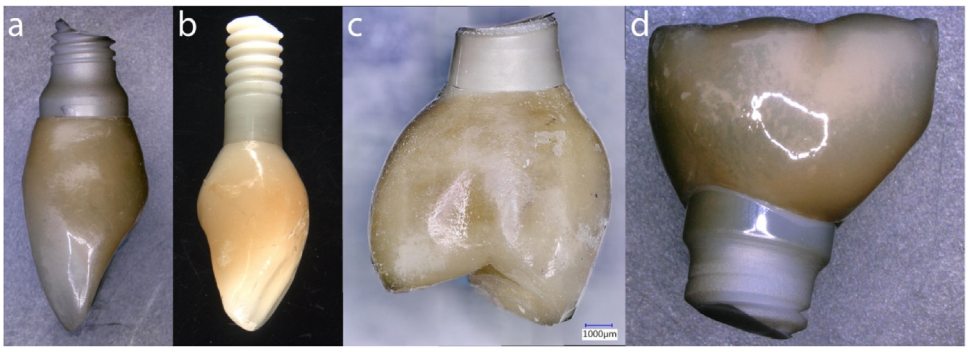

Fig. 1 – One example per manufacturer of a recovered crown-implant part: (a) Z-Look 3 (Z- Systems); (b) PURE Ceramic implant (Straumann); (c) AXIS Integra Monobloc (Axis Biodental); (d) SDS 1.0 TZP CD (Swiss Dental Solutions). Crown-implant parts in Fig. 1a, c and d are slightly gold-coated.

tographic analysis, it is more difficult to assess how occlusion and off-axis loading may contribute to a specific case of premature implant fracture.

In that respect, the purpose of this paper was to take advantage of recovered broken zirconia implants parts with their cemented crown on top to perform not only a full fractographic failure analysis but also to integrate in a mathematical model the spatial coordinates obtained from 2D and 3D images of the crown-implant part. The model created should provide a basis for understanding and visualizing the immediate effect of loading one occlusal contact more than another on the resultant bending moment, generated stress and calculated crack onset location on the implant. A matching of the location of the crack onset on the implant with that of the identified origin from fractographic analysis would show which occlusal contact has been dominantly loaded contributing to the zirconia implant fracture.

2. Materials and methods

2.1. *Recovered fractured implant parts*

A total of 15 broken zirconia implant parts (11 posterior and 4 anterior) with their crowns still cemented on it were recovered by the treating dentists in 4 private dental offices in Switzerland and Germany and from a university-based clinic (Geneva, Switzerland) and donated to the prime investigator of this paper for failure analysis. The recovered parts consisted of the upper broken implant portion with its cemented crown (Fig. 1). These first generation monotype zirconia implants were made of 3Y-TZP from four manufacturers, AXIS Biodental, Z-Systems, Straumann and Swiss Dental Solutions (SDS) with different processing and surface treatments. Table 1 summarizes the recovered material available including implant labelling, FDI location, implant's surface treatment, time-to-failure, brand name, diameter and manufacturer. The time-to-failure varied from 2 weeks to 9 years of intra-oral function.

AXIS Biodental uses an injection molding process for their zirconia implants and has the CE label for it. The addition in 2008 of a proprietary porous zirconia coating (patent EP 1924300 B1) added to the injection molded implant in the partially sintered state before densely sintering and hot isostatic pressing was intended to increase the surface roughness and favor faster bone integration. To test this coating, a one year multicentric preclinical trial was launched by the manufacturer in 2008 and announced to SwissMedic (2008-MD-0007) after receiving approval of the local ethic committee (PSY 08-036). The multicentric trial involved two private practices in Switzerland and one university-based clinic (University Clinic of Dental Medicine in Geneva). After one year of intra-oral function, 6 from 33 posterior 3Y-TZP implants had fractured (in two private offices). These negative results were summarized in a manufacturer's report to SwissMedic in 2011, at the end of the one year preclinical trial. The coating was abandoned in the same year and the manufacturer went back to the production of his original injection molded implant. During the following seven years four more implants fractured from this trial (2 from the University clinic and 2 from a private practice) and were donated to the prime investigator of this paper. Therefore, as of 2018, a total of 10 recovered fractured posterior AXIS Integra Monobloc implants inserted between 2008–2010 were analyzed with times-to-failure varying from 2 weeks up to 8 years of survival (Table 1). Fig. 2 illustrates such an in situ fractured zirconia implant on a second lower left molar (#37) 3 weeks after intraoral loading of the cemented all-ceramic crown which was made of a zirconia framework and layered with a veneering leucite-based ceramic. An open gingival flap exposes the broken implant part still in the bone (Fig. 2b). Fig. 2c shows the X-rays of the implant with its restoration after cementation (left) and after fracture (right). The dotted line on the left X-ray indicates the level of fracture located between two threads adjacent to the bone level.

Three central incisors implants fractured were Z-Look 3 (Z-Systems), from a first generation of reduced diameter (3.25 mm) implants. The surface treatment of these implants was sandblasting with large-grit alumina particles (>100 µm). The failure case at 9 years (ZS 11-9y) occurred during the retrieval of a silicon impression in a patient to restore the neighboring implant. The two others cases which failed after 2 years and 5 years (ZS 11-2y and ZS 21-5y) were part of a clinical study [27,28] and fractured during function with no special chewing event.

The lateral upper incisor fractured implant was of reduced diameter (3.3 mm) and on the market since 2014 (PURE

Table 1 – Recovered fractured zirconia implants for failure analysis. Surface treatments: porous coating (pc), large grit alumina particle sandblasting (SbA), zirconia sandblasting (SbZ), alumina sandblasting followed by acid-etching (ZLA).

Implant label	Implant FDI #	Surf. ttt	Time to failure (months)	Brand name and implant diameter (mm)	Manufacturer
AXIS 15-2w	15	pc	0.5	Monobloc Integra (Ø 4.1)	Axis Biodental; Les Bois; CH
AXIS 37-3w	37	pc	0.75	Monobloc Integra (Ø 4.1)	Axis Biodental
AXIS 15-3m	15	pc	3	Monobloc Integra (Ø 4.1)	Axis Biodental
AXIS 45-4m	45	pc	4	Monobloc Integra (Ø 4.1)	Axis Biodental
AXIS 14-6m	14	pc	6	Monobloc Integra (Ø 4.1)	Axis Biodental
AXIS 44-8m	44	pc	8	Monobloc Integra (Ø 4.1)	Axis Biodental
AXIS 35-4y	35	pc	44	Monobloc Integra (Ø 4.1)	Axis Biodental
AXIS 25-6y	25	pc	75	Monobloc Integra (Ø 4.1)	Axis Biodental
AXIS 36-7y	36	pc	83	Monobloc Integra (Ø 4.1)	Axis Biodental
AXIS 26-8y	26	pc	98	Monobloc Integra (Ø 4.1)	Axis Biodental
ZS 11-2y	11	SbA	25	Z-Look 3 (Ø 3.25)	Z-Systems; Oensingen; CH
ZS 21-5y	21	SbA	69	Z-Look 3 (Ø 3.25)	Z-Systems
ZS 11-9y	11	SbA	108	Z-Look 3 (Ø 3.25)	Z-Systems
PURE 22-1y	22	ZLA	18	PURE Ceramic (Ø 3.3)	Straumann; Basel; CH
SDS 46-1m	46	SbZ	1	SDS 1.0 TZP CD (Ø 5.0)	Swiss Dental Solutions; Kreuzlingen; CH

Ceramic Implant, Straumann). The implant's surface underwent a proprietary sandblasted and acid-etching treatment (ZLA) in order to reproduce a similar surface texture as with the Titanium SLA implants. This failure case occurred after 18 months in a patient with heavy bruxing habits and, unlike the other fractures, failed between the 5th and the 6th thread, approximately 5 mm inside the bone (Fig. 3).

The recovered broken implant part, a SDS 1.0 TZP CD (Swiss Dental Solutions) implant of 5.0 mm diameter placed on a first lower molar was also from a first generation of 3Y-TZP HIPed implant on the market between 2009 and 2012 and inserted in a private practice end of 2012. This implant was discontinued in 2013 and replaced with novel designs and surface treatment of 3Y-TZP HIPed zirconia implants.

All available X-rays, showed fracture of the implants at the crestal bone level (Fig. 2c) except for the PURE Ceramic implant which fractured approximately 5 mm inside the bone (Fig. 3).

2.2. *Fractographic failure analyses*

A systematic approach using both, a digital microscope (Keyence VHX 5000, Keyence International, Mechelen, Belgium) and a FE-SEM (Sigma 300 VP, Zeiss, Oberkochen, Germany) was performed on all broken implants. The recovered implant-crown parts were cleaned in an ultrasonic bath with sodium hypochlorite (5%) followed by pure ethanol before being lightly gold-coated (20 nm) to enhance reflectivity for improved imaging. Fracture surfaces were first photographed with a digital microscope to search for easy detectable macrostructures such as a compression curl, arrest lines and large twist hackle for the direction of crack propagation (dcp). Further SEM investigation searched for more details regarding surface flaws, critical crack sizes at the origin, microstructural inclusions, as well as transgranular or intergranular crack propagation. The implants outer surfaces were investigated regarding texture and microstructure. The occlusal crown's surface was photographed both with the digital microscope and SEM for occlusal contact wear locations. Zones with larger wear pattern were considered receiving higher mastication loads.

2.3. *Calculations for M_t, M_b, τ, σ, σ_{max} and von Mises stress equivalents*

All posterior fractured implants (10 AXIS and 1 SDS) were used for calculation of resultant torsion and bending moments (M_t, M_b), corresponding shear (τ) and tensile (σ) stresses, maximum principal stress (σ_{max}) as well as von Mises stress.

As a first step, the implant-crown part was defined in space (Fig. 4a) O,X,Y,Z for which OZ is the implant's central axis and O the intersection of Z with the implant's fracture surface. An arbitrary easy to recognize detail on the occlusal surface was used as a reference point (R) in the O,X,Z reference plane (Ref., yellow). On the crown's occlusal surface, Ci corresponds to the center of an identified occlusal contact area. A plane, Pi (white), goes through O,Xi,Z and Ci. The hypothesis was made, that the applied load was normal in each contact point. In that respect, the green arrow (n_i) represents the vector normal to the occlusal contact surface in C_i.

In a second step, the crown-implant was photographed with a digital microscope in 2D and 3D in order to measure coordinates for bending moments. For that, the crown-implant part was positioned vertically in a cylindrical flat-base holder containing a centered hole fitting the implant's neck up to the junction with the crown's margin, so that the implant's axis (OZ) is normal to the base of the holder. In this centered position, the occlusal surface of the crown and the flat base of the holder were photographed with the digital microscope in a 2D and 3D mode. On the 2D image (Fig. 4b), the implant's central axis intersecting with the occlusal surface (black–white dot) and the implant's outer diameter (dashed circle) were determined. Using the microscope's software, distances and angles were measured connecting the implant's center (black–white dot) with the center of identified occlusal contacts (numbered black dots) and an arbitrary reference (black star, Ref.). On lateral views of the crown-implant part, the distance (h) from the neck's shoulder to the fracture origin as well as the width (w) of the implant at the fracture site (Fig. 4c) were measured. From the 3D image, the orientation and location of the vector (n_i) normal to C_i was determined.

A mathematical model spreadsheet was created containing cells integrating all measured coordinates and extracted

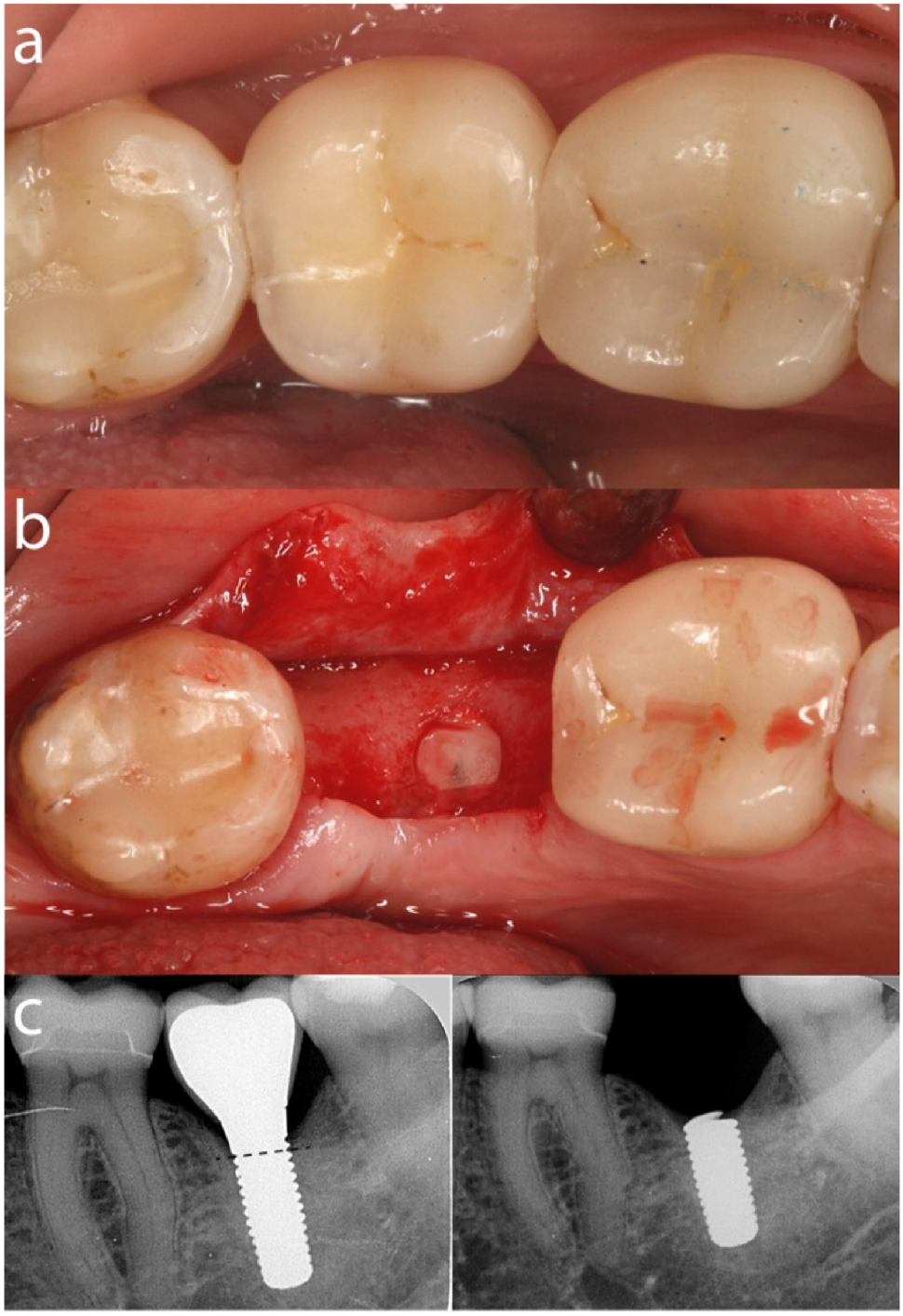

Fig. 2 – (a) Clinical image of the ceramic crown cemented over a 3Y-TZP implant (AXIS Biodental) on the second lower left molar (tooth FDI # 37); (b) fracture in situ of the zirconia implant at the bone level. A flap is open to expose the implant part still in the bone; (c) X-ray of the implant #37 with its restoration after cementation (left) and after fracture (right). The dotted line indicates the level of fracture at the crestal bone level. The fracture occurred 3 weeks after intraoral loading of the crown.

data from the 2D and 3D images of the crown-implant part. The mathematical spreadsheet contained all the needed equations for calculations of moments and stresses (Appendix A). In order to generate bending and stress values, the mathematical model requests information on the applied load in each identified occlusal contact (Ci). For that purpose, a total occlusal load of 500 N distributed over the contacts was selected based on maximum biting forces reported for implant supported restorations [29]. How much of the 500 N loads would be allocated for each occlusal contact was based on wear evidence (surface and roughness appearance on the SEM images). Large roughened ceramic surfaces would be considered as primary or dominant contacts (red circle in Fig. 4b) with approximately 80% of the total load distributed. Smaller (i.e.

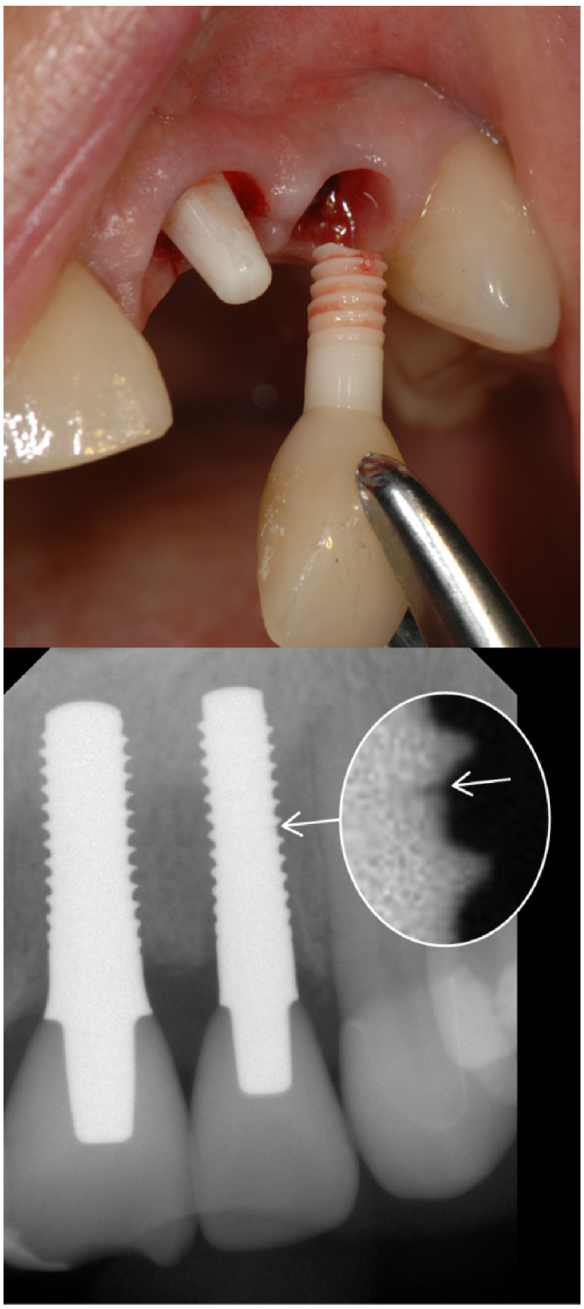

Fig. 3 – Retrieval of the broken PURE Ceramic zirconia implant after 18 months of intraoral loading. The white arrow on the X-ray taken before retrieval shows the location of the fracture seen on the contrast-modified and enlarged digital image (medallion).

secondary) contacts (green circles) would receive the remnant 20% of loading.

Based on the occlusal load distribution and the resultant bending moment, the model provided also an angular position (white arrow) from the occlusal arbitrary reference (Ref.) of the crack onset on the implant's fracture surface (Fig. 4b). This location would be compared with the original fracture origin (O) determined from fractographic analysis. Occlusal contact loads would be fine-tuned to generate an angular position of the crack onset that would match as close as possible the fracture origin determined from fractography.

3. Results

3.1. *Fractography*

A first general failure analysis was performed at low magnification (20–30×) with the digital microscope. Fig. 5 illustrates representative zirconia implant fracture surfaces (a = SDS; b = PURE Ceramic Implant; c = Z-Systems (ZS); d–f = AXIS). A thin layer of gold-coating enhanced the fracture surface features. All 15 implants had an easily recognizable macrostructure which is the compression curl marked by an asterisk. This curl is created when a propagating crack enters a compression stress zone and is typical for bending or flexure fractures. The opposite side to the compression curl is where the fracture origin is located (arrow). In all 15 recovered implants, the crack originated in the constriction region between two threads, where the section of the implant is the narrowest.

Multiple larger twist hackle (th) have formed along the implant's fracture surface periphery within 1–2 mm next to the origin in all AXIS implants as seen in Figs. 5d–f. Concentric arrest lines (ar) (Fig. 5d) formed up to 300 μm above the origin, are indicators of cyclic loading in flexure and were seen exclusively in AXIS implants. The presence of arrest lines is due to slight variation in the crack growth plane. The fracture surfaces for SDS (a) and AXIS (d–f) appear rather smooth. They are made of very fine hackle, compared to PURE Ceramic implant (b) and Z-Look 3 (Z-Systems) (c), both showing a more textured, rough surface with coarser hackle radiating from the origin.

3.1.1. *AXIS implants*

The following SEM images show the area related to the crack origin (O) at lower and higher magnifications, as well as the direction of crack propagation (dcp). For all AXIS implants, the porous and cracked zirconia coating is intimately involved in the fracture origin (O) as shown in Fig. 6a,c,e. Several starter cracks (small white arrows) next to larger twist hackle (th) are visible on the periphery of the implant's fracture surface in the vicinity of the main origin (O). Twist hackle is a hackle that underwent a twist when the axis of principal stress slightly tilts. The running crack, in response to the new stress direction, breaks into small unconnected segments each of which is separated by larger steps. Arrest lines are visible in Fig. 6e indicating episodes of a crack which is momentarily brought to a halt before it continues to propagate under a slightly different stress configuration. The higher magnifications (Fig. 6b,d,f) show close-ups of the origin connected to the porous coating which is 12–30 μm thick (*a*) at the fracture origin site.

Fig. 7 illustrates an AXIS implant which broke after only 2 weeks of intraoral loading (AXIS 15–2 w). All the classic fractographic features are visible. The origin (O) (white arrow) in the center has many neighboring twist hackle spread over 2 mm along the implant's fracture surface periphery. Several arrest lines (ar) are clearly visible up to 300 μm above the origin. Small twist hackle are radiating out like a fan from the

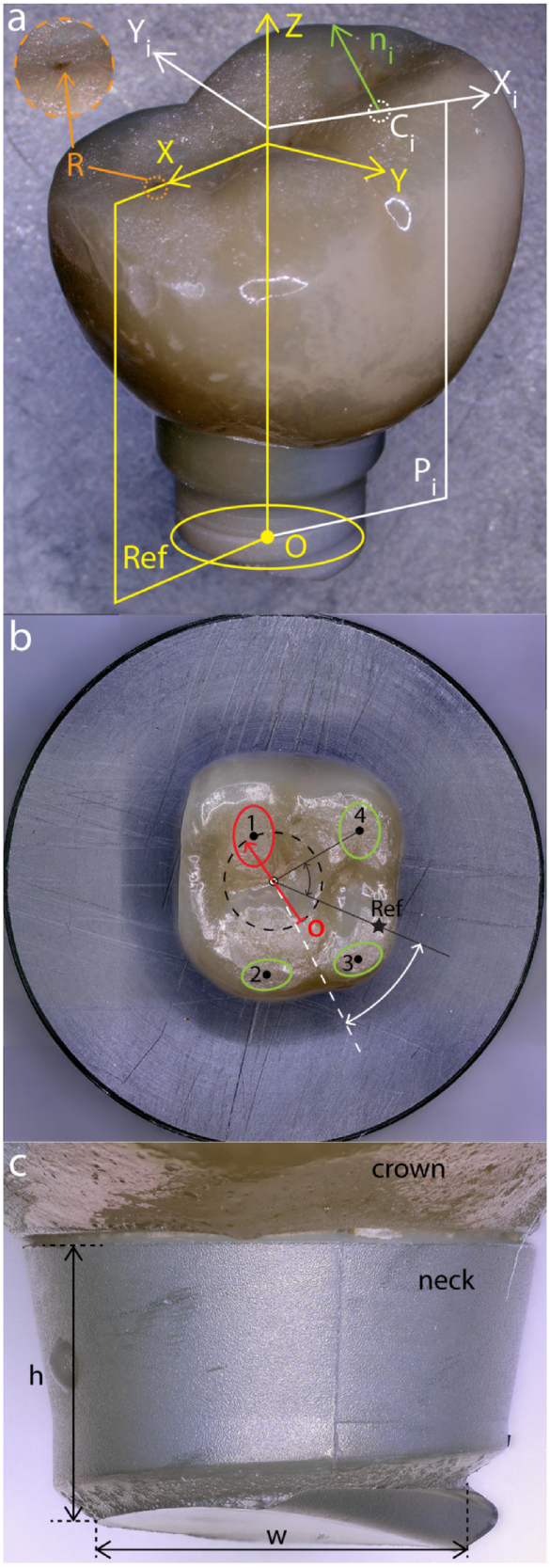

Fig. 4 – Schematic representation of the spatial coordinates and references of the crown-implant part. Fig. 4a: Reference planes and force vectors: OZ implant's central axis; (R) arbitrary reference on the occlusal crown's surface; (Ref.) implant's reference plane (yellow); (C_i) center of occlusal contacts, (P_i) plane going through C_i and OZ; (n_i) (green arrow) vector normal to the occlusal crown's surface in C_i. Fig. 4b: 2D image of the crown's occlusal surface for which the implant's neck (i.e. implant's axis) is positioned perpendicular to the holder's flat base. The implant's center (black-white dot), outer implant's diameter (dashed circle), identified Ci's (numbered black dots), and an arbitrarily chosen reference (Ref.) (star) are marked. Angles and distances connecting the reference and occlusal contacts to the projected implant's center are measured. Red circle corresponds to dominant wear occlusal contact and green circles to lighter contacts. The calculated angular position of the crack onset is indicated with the white arrow. The red arrow illustrates the crack propagation direction and location of the crack origin (O) as determined from fractographic findings. Fig. 4c: side view of the implant's neck with measurements of height (h) from the implant's neck to the fracture origin and width (w) of the implant (inner diameter) at fracture. (For interpretation of the references to colour in this figure legend, the reader is referred to the web version of this article.).

densely sintered zirconia implant at the junction with the porous coating (Fig. 7b). The porous coating (pc) at the fracture origin has an approximate thickness of 36 μm (*a1*). A closer look at the microstructure in fig. c shows a transgranular fracture surface (fs) within the implant's bulk, whereas the grains of the porous coating are round, from free-air sintering (Fig. 7c,d). This occurs if a crack is present in the coating and created during processing of the coating prior to dense sintering. An attempt to calculate the stress at fracture can be done using the critical crack size and shape and applying the fracture mechanics equation of $K_{Ic} = Y\,\sigma\,\sqrt{a}$ (Eq. (1)). Considering $a2 = 44$ μm as the critical crack, a corresponding stress intensity shape factor $Y = 1.3$ for a semi-circular crack shape (white arrows in Fig.b) and assuming a toughness $K_{Ic} = 5.0$ for 3Y-TZP, the calculated fracture stress (σ) would be 580 MPa. If however we consider the coating thickness as the critical crack ($a1 = 36$ μm) with its corresponding semi-elliptical Y shape factor of 1.6, then the fracture stress (σ) would be 520 MPa. The cracks within the coating were often reaching the implant's injection molded bulk (Fig. 7b). A partial gap between the porous zirconia coating and the densely sintered zirconia body is seen in Fig. 7c at the fracture origin site.

3.1.2. *Z-Systems*

Two cases central incisors broken implants of reduced diameter (3.25 mm) after 2 and 5 years are illustrated for Z-Look 3. Fig. 8a (ZS 11-2y) shows classic fractographic features such as hackle and twist hackle (th) easily recognizable on the fracture surface and indicating the dcp. The origin (O) marked with an arrow starts at the periphery of the implant which contains many deep and sharp cuts (Fig. 8b,c) from large grit (>100 μm) alumina particles sandblasting. Fig. 9 of a fracture after 5 years (ZS 21-5y) is similar with a fracture origin connected to deep grooves on the outer implant sandblasted surface (Fig. 9c,d). Along the implant's fracture surface periphery, close to the

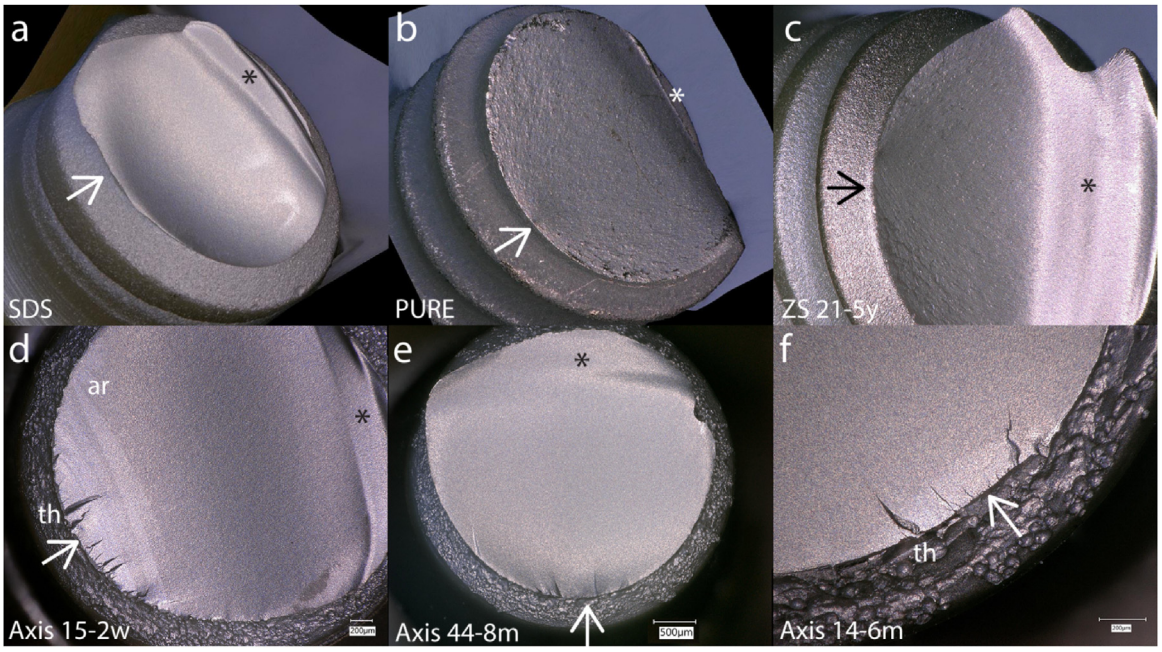

Fig. 5 – Implant fracture surface: a = SDS; b = PURE Ceramic Implant; c = Z-Systems; d,e,f = AXIS. The compression curl is marked by an asterisk (*). The fracture origin is marked by an arrow. AXIS fractured surfaces (Fig. 5d,e,f) show several vertical lines called twist hackle (th) starting along the implant's fracture surface edge in the vicinity of the origin over a distance of 1–2 mm. Several arrest lines (ar) (Fig. 5d) (horizontal lines above the origin) can be visualized for AXIS broken implants.

origin, microcracks (Fig. 10) running downwards to the apex of the implant may have been created by cyclic fatigue loading. Both of these cracks, however, were not involved in the failure origin but denote that the implant has suffered during intraoral function.

3.1.3. *PURE Ceramic implant (Straumann)*

The PURE Ceramic implant fracture on a lateral incisor occurred deeply inside the bone at a very unusual location. Fig. 11 illustrates the fracture origin (O) location at the periphery with hackle radiating out in the direction of crack propagation (black arrows). Higher magnifications in Fig. 11b,c show an origin masked by friction patterns which are also visible approximately 400 μm above the fracture origin (Fig. 11d). It is hypothesized, that when the sudden fracture occurred, the broken implant parts rubbed against each other.

3.1.4. *SDS*

Fig. 12 illustrates the SDS implant which fractured after 1 month. The overall view (a) shows the crack propagation direction (dcp), the compression curl (*) and the fracture origin location (O, white arrow). The higher magnification of the fracture origin (Fig. e) measures a critical crack depth (*a*) of approximately 36 μm and a width of approx. 80 μm. This gives a semicircular Y shape factor of 1.3. Assuming a K_{Ic} of 5.0 for 3Y-TZP zirconia, the corresponding fracture stress would be 641 MPa (Eq. (1)). The implant's outer surface has a microroughened aspect from zirconia particle sandblasting by the manufacturer (Fig. 12a,b,d) and is made of fine (<500 nm) free-air sintered zirconia grains (Fig. 12c).

3.1.5. *Fracture surface microstructure*

The crack propagation through the microstructure was observed for all implants. All implant's fractured surfaces showed a mixed mode of transgranular and intergranular fracture path cleaving the grains (Figs. 13 and 14a,d). At 20,000× some twinning is recognizable by the step-like pattern of transformed zirconia grains is seen in Fig. 13b. Localized extensive grain growth, possibly cubic zirconia was seen on the fracture surfaces of Z-Systems and PURE Ceramic implants (Fig. 14a) as well as on the acid-etched outer implant surface (Fig. 14b). Large (2–4 μm) alumina particles (Fig. 14c,d) randomly distributed were detected and confirmed by EDX on the fracture surface of all Z-Systems implants.

3.1.6. *Occlusal contact wear*

Similar wear patterns have been noticed on the occlusal surfaces of the ceramic crown restorations recovered with the fractured implants parts. The ceramic crowns on AXIS, Z-Systems and SDS had a zirconia framework and were veneered with a leucite-based ceramic. The crown on the PURE Ceramic implant was a lithium disilicate restoration. Fig. 15a,c,d (AXIS 26-8y) illustrate with increasing magnifications the localized mesio-buccal occlusal wear surface generated after 8 years of intraoral function. This surface corresponds to contact 1 illustrated in Fig. 3. The wear facet in Fig. 15a, is the result of contact wear during lateral (*i.e.* buccal) excursions as seen by the concave fractured areas. Higher magnifications (Fig. 15c,d) show the brittle fracture behavior of the veneering leucite-based ceramic under contact loading and sliding motion with extensive microcracking. Fig. 15b shows a similar wear patter on the incisal edge of a lithium disilicate ceramic restoration after 18 months (PURE Ceramic Implant). Both cases (Fig. 15a,b)

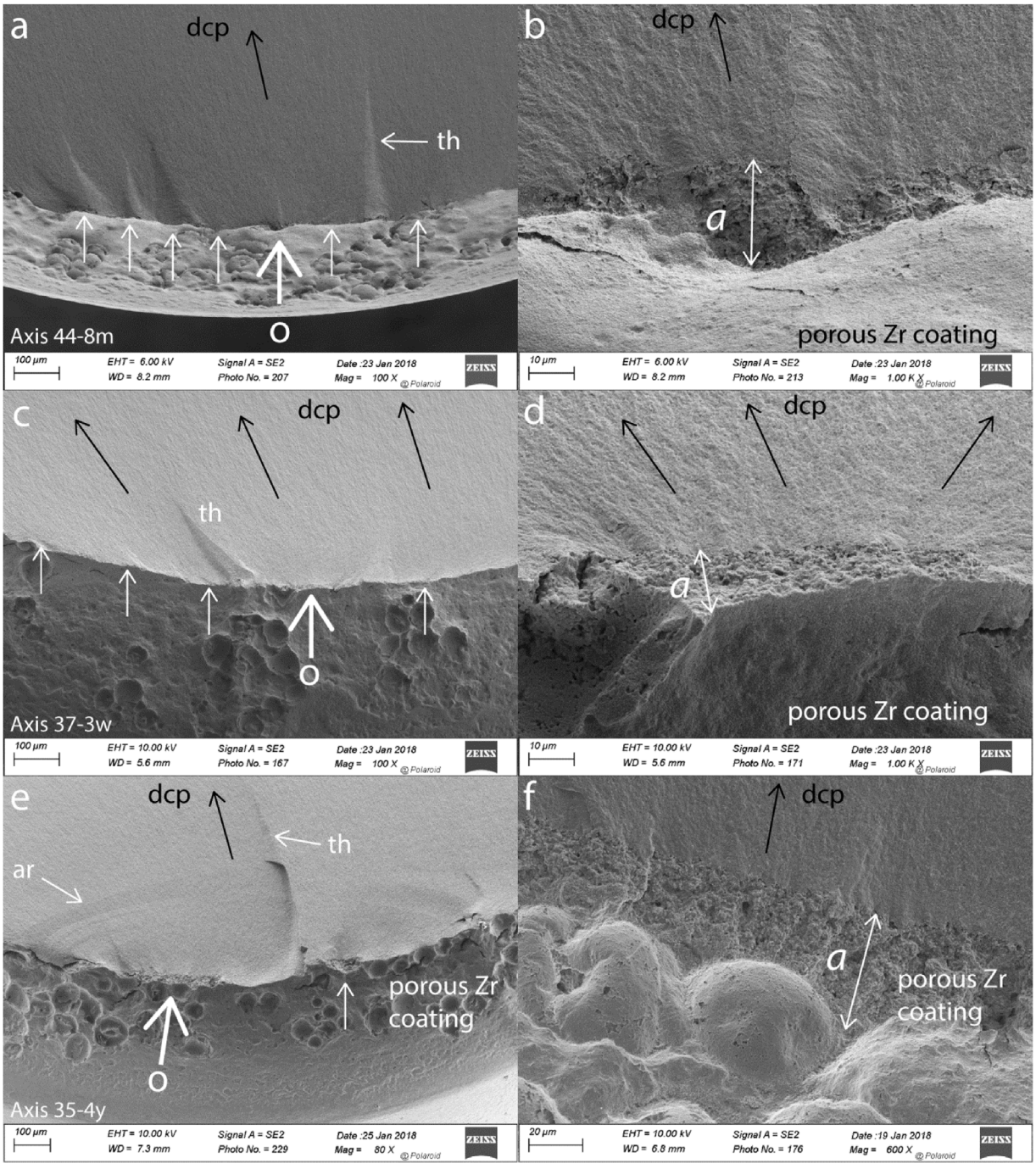

Fig. 6 – Fractographic analyses of three AXIS implants failed after 8 months (a), 3 weeks (c) and 4 years (e). At lower magnification (left images), the origin (O) is surrounded by several other smaller starter cracks (light white arrows) next to larger twist hackle (th). Several arrest lines (ar) are visible in Fig. 6e. The respective higher magnifications (Fig. 6b,d,f) show the origin next to the porous zirconia coating which is between 12 and 30 μm thick (*a*).

show similar brittle fracture behavior of the ceramic undergoing contact wear during function.

3.2. *Bending and torsion moments and resulting stresses*

Table 2 provides all the calculated values of resultant bending (Mb) and torsion (Mt) moments, respective shear (τ), tension (σ), maximum principal stresses (σ_{max}) and von Mises equivalent (vM), based on a total load of 500N distributed over identified occlusal contacts. Location of the crack onset (see also Fig. 4b) is given by an angular position (A°) with respect to the arbitrary reference (*) (Fig. 16). Negative angles are clockwise from the reference; positive angles are counterclock wise from the reference. The loads for each selected occlusal contact were chosen based on the severity of wear seen under

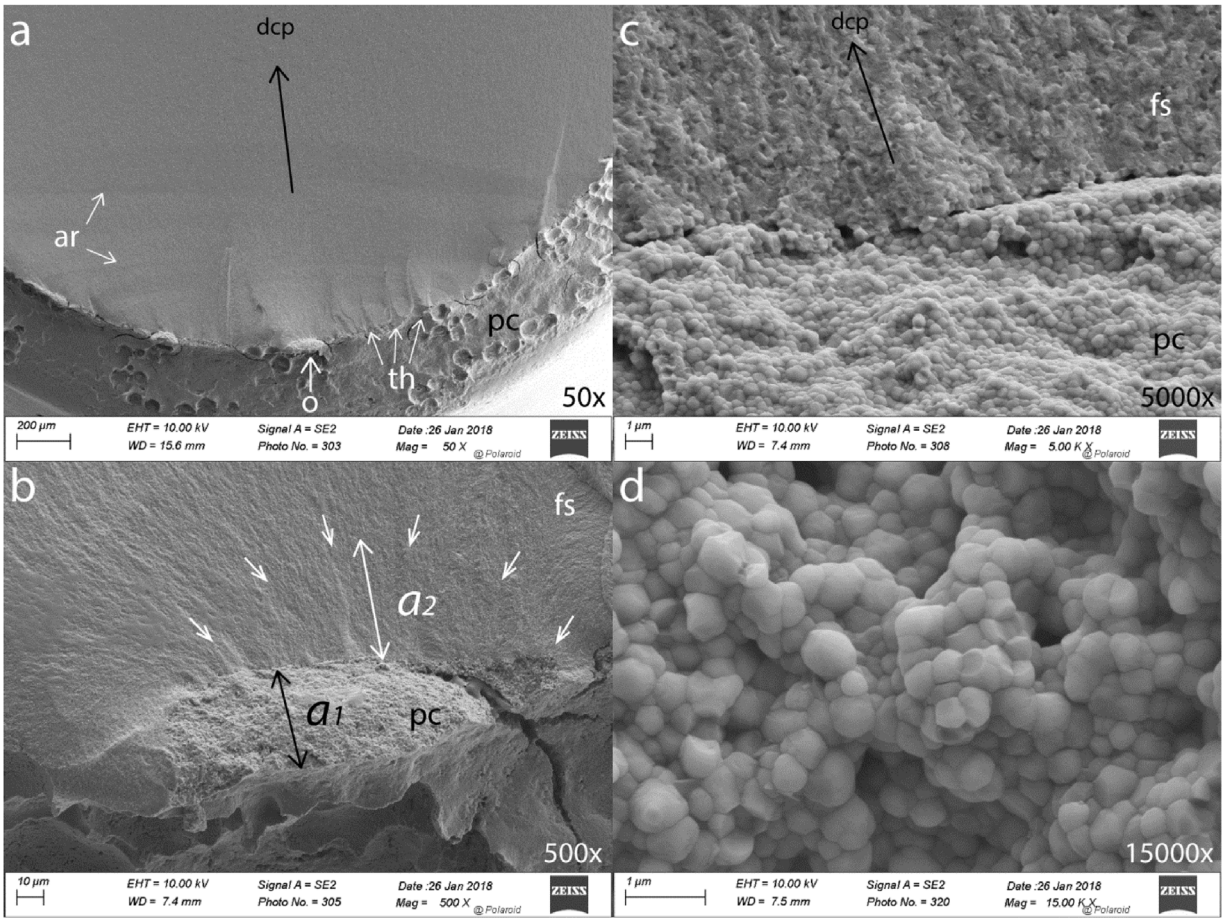

Fig. 7 – AXIS 15-2w: Fig. 7a: Fracture origin (O), arrest lines (ar), many twist hackle (th) and dcp. Fig. 7b is a higher magnification of the fracture origin region in Fig. 7a. The porous coating is of approx. 36 μm in depth (*a*1) at the crack initiation site. The critical crack (*a*2) is in the bulk next to the porous coating and measures approx. 44 μm in depth (semi-circular crack shape marked with white arrows). Small twist hackle are emanating like a fan from that junction. Fig. 7c is a higher mag of Fig. 7b of the junction between the fracture surface (fs) of the zirconia bulk implant and the porous coating. The grains throughout the pc thickness (*a*1) are round and thus free-air sintered (Fig. 7d) indicating an already existing crack in the coating before dense sintering.

Table 2 – Resultant bending (M_b) and torsion (M_t) moments with respective shear (τ), tension (σ), maximum principal stresses (σ_{max}) and von Mises (vM), based on a total load of 500 N distributed over identified occlusal contacts. Location of the starter crack is given by an angular position (A°) with respect to the arbitrary reference (*). Negative angles are clockwise from the reference; positive angles are counterclock wise from the reference * (see Fig. 16 for occlusal contact numbering).

Implant label	Distributed 500 N load over identified occlusal contacts (see Fig. 16)					M_t Nmm	M_b Nmm	Shear (τ) MPa	Tension (σ) MPa	σ_{max} MPa	v. M. MPa	A °
	1	2	3	4	5							
AXIS 15-2w	50	50	350	50	–	50	1959	6.5	508	508	508	−87
AXIS 37-3w	450	40	5	5	–	101	2706	13	701	701	701	−178
AXIS 15-3m	175	25	250	50		−29	1324	3.7	343	343	343	43
AXIS 45-4m	5	5	20	120	350	−464	2016	60	523	529	533	162
AXIS 14-6m	25	450	25	–	–	877	1523	124	432	464	482	2
AXIS 44-8m	20	50	75	350	5	61	654	8.7	185	186	186	139
AXIS 35-4y	155	45	250	25	25	296	815	41	231	238	242	−1
AXIS 25-6y	300	160	20	20	–	17.5	1291	2.5	366	366	366	−68
AXIS 36-7y	200	100	100	50	50	−95	1452	12.3	376	377	377	60
AXIS 26-8y	375	75	25	25		139	1879	18	487	488	488	−40
SDS 46-1m	100	200	25	25	150	−229	1741	21	323	325	325	15

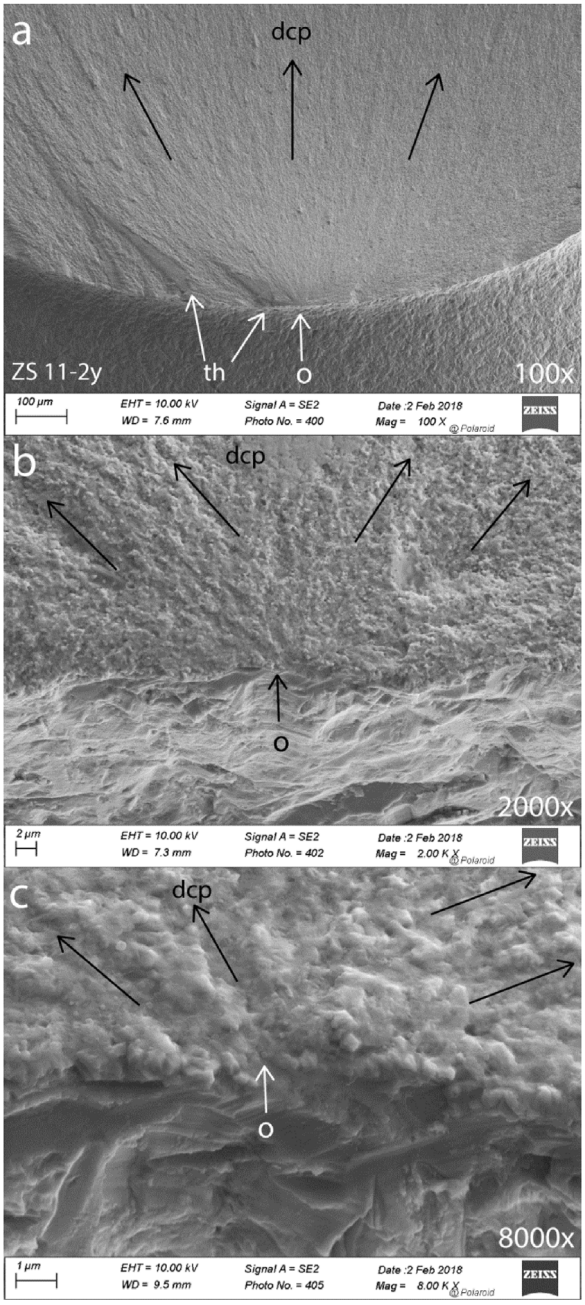

Fig. 8 – Z-Systems (ZS 11-2y). Fig. 8a is an overall view at 100× magnification in which large twist hackle (th) are visible next to the fracture origin (O). The direction of crack propagation (dcp) is indicated by the black arrows. Higher magnifications of the fracture origin are shown in Fig. 8b,c. The external implant surface shows deep cuts from alumina sandblasting which are connected to the fracture origin (Fig. 8c).

the microscope and for which the calculated angular position (A°) would match closely that of the true fracture origin. Tension and von Mises stresses are identical if the shear stress is small. Hence, the only case in which the shear stress played a role was AXIS 14–6 m (Fig. 16e) as the main contact (number 2) was on the mesial crest and modelled with 450 N. The resultant angular position of 2° was close to the real fracture origin location. This induced a shear stress of 124 MPa resulting in higher von Mises stress (482 MPa) than the normal tension stress (432 MPa).

The digital images in 2D of Fig. 16 illustrate the findings in Table 2 for the 11 posterior implant fracture cases. The projected implant center (black dot) and diameter at fracture (dashed-line circle) are marked on the occlusal crown surface. The identified occlusal contacts on which the 500 N loads are distributed are numbered. Red circles represent main occlusal contacts receiving high mastication load, whereas green circles represent lighter contact. The star (*) corresponds to the arbitrarily chosen reference. The current selected loads and distribution (Table 2) come to a close match between the true

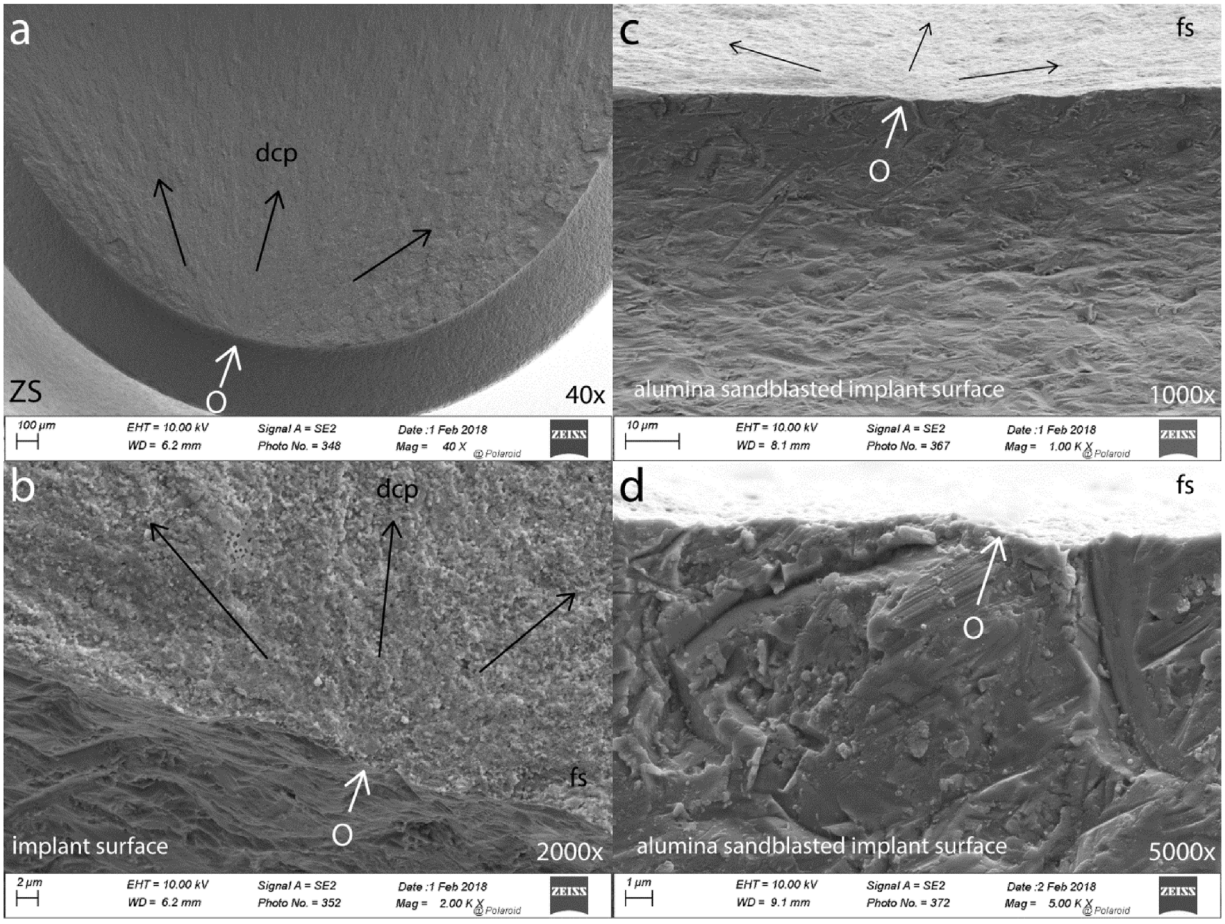

Fig. 9 – Z-Systems (ZS 21-5y) implant fracture of a central incisor after 5 years. Fig. 9a shows the fracture surface (fs) at low magnification (40×). The origin (O) is marked by a white arrow and the dcp is indicated with black arrows. Fig. 9b is a 2000× magnification of Fig. 9a of the fracture origin region. The implant's outer surface is rough from alumina sandblasting. Fig. 9c and d show side views of the sandblasted implant's outer surface next to the fracture origin. At 5000× magnification (Fig. 9d), deep sharp cuts created by the alumina particle sandblasting are connecting with the fracture origin (O).

fracture origin location (starting point of the red arrow indicating the crack propagation direction) and the calculated crack onset location. Fine-tuning of the applied load in each contact was performed with the mathematical model in order to match both A° and the fracture origin location. An example is given for the implant AXIS 36-7y (Table 2, Fig. 16a1). Strong wear was seen in contact points 1–3. The loads were therefore distributed with 200 N in point 1 (strong wear surface), 100 N in point 2 and 100 N in point 3. Additional loads of 50 N were distributed in each of the remaining buccal lighter contact points 4 and 5. With this distribution the fracture origin location matched with the calculated angular position of 60° (counterclock) from the reference point (black star). Another example is illustrated in Fig. 16h1–h2, the implant's axis is located bucco-mesially and off-centered. The mesial veneering ceramic had chipped off therefore an important load was modeled in this region marked with a red contact (3). A second strong load was inserted on the tip of the palatal cusp (contact 1) marked by occlusal adjustments. This loading choice provided a good match between the calculated angular position of the crack onset (43°, Table 2) and the fracture initiation site determined from fractography (Fig. 16h1, beginning of red arrow).

An example of how loading of the occlusal contacts affects the angular position of the starter crack is illustrated in Fig. 17, representing the case of AXIS 26–28 years. As reported in Table 2 and Fig. 16g, the selected contacts had a load distribution of 375 N, 75 N, 25 N and 25 N, for which an angular position of −40° was calculated matching nicely the fracture origin location (O). If the loads are changed to a distribution of 250 N, 150 N, 50 N, 50 N, the calculated angular position of the crack initiation would be −52° moving away from the true fracture origin. Thus the red circled zone (mesio-buccal cusp) represents the prime contact receiving 75% (375 N) of the total 500 N load distribution in order to create a resultant bending moment with a critical stress concentration and crack onset near the true fracture origin.

Three out of 4 anterior zirconia implants failed as expected from palatal towards buccal, due to contact loading of the upper central incisal palatal surface of the crown. The vector force applied was in the buccal direction putting the palatal implant surface in tension. The only exception to this palatal fracture origin was the Z-Look 3 implant (ZS 11-9y) which

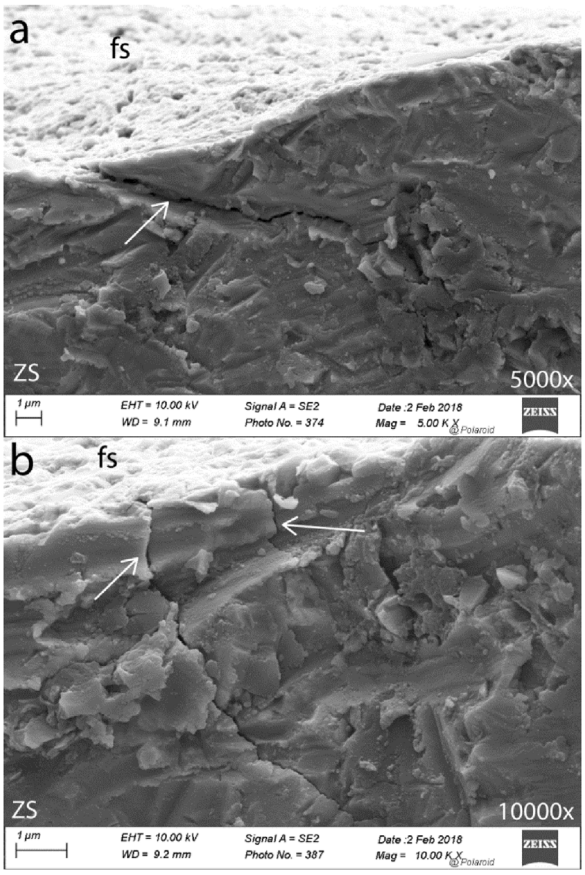

Fig. 10 – Z-System (ZS 21-5y). Along the implant's fracture surface periphery, close to the origin, microcracks are running downwards to the apex of the implant. These cracks may have originated during cyclic loading. Both of these cracks, however, were not involved in the failure origin but denote that the implant has suffered during intra-oral function.

broke from buccal to palatal during the retrieval of a silicon impression. A dislodging force exercised from the incisal edge towards palatal created tension on the buccal implant surface from where fracture started. Such rare event, however, reminds us that ceramic does not deform plastically and that any forceful dislodging movement has to be done with a direction of retrieval in the main axis of the crown.

4. Discussion

The purpose of this research paper was to extract as much scientific information as possible out of 15 clinically broken zirconia implants for which the upper parts were recovered with their cemented restorative ceramic crowns. The innovation of this research was to include in the fractographic failure analysis a mathematical model integrating the location of occlusal contacts on the crown's surface with respect to the central axis of the implant. The model, which contained all spatial crown-implant coordinates obtained from 2D and 3D images, not only provided calculations of bending and torsion moments but also angular positions of the crack onset location on the implants. By fine-tuning the loads on the identified occlusal contacts, a close match of the calculated crack onset and the fracture origin was reached. Hence, for all 11 posterior fracture cases, the prime loading region on the crowns were identified and visualized with respect to their implant's central axis and fracture origin. The mathematical model together with the 2D images was helpful in showing how occlusal loading affects the location of the fracture initiation site on real clinical zirconia implant fracture cases. It is important to visualize that the implant's center may not necessarily correspond to the center of the crown and that occlusal contacts may be quite off-centered thus generating increased bending of the structure. The model can be adapted and include as many contacts as identified. The clinician, inspecting the crown's occlusal surface under a microscope decides which contact would be primarily loaded based on wear evidences. For a clinician, such information is important as it highlights the influence of loading occlusal contacts on bending moments, stress concentrations and crack onset location.

The limitations of our contact load modelling can be summarized as follows. Firstly, it was difficult to identify occlusal contacts from wear evidence on crowns on which occlusal adjustments had been made as some roughness from polishing overlapped localized contact wear. Clinical pictures of color-marked occlusal contacts would have been helpful. Secondly, we used maximum biting forces of 500 N [29] reported for implant supported crowns and distributed these over the contacts integrating wear information. Therefore, the values in Table 2 should by no means be considered as true values

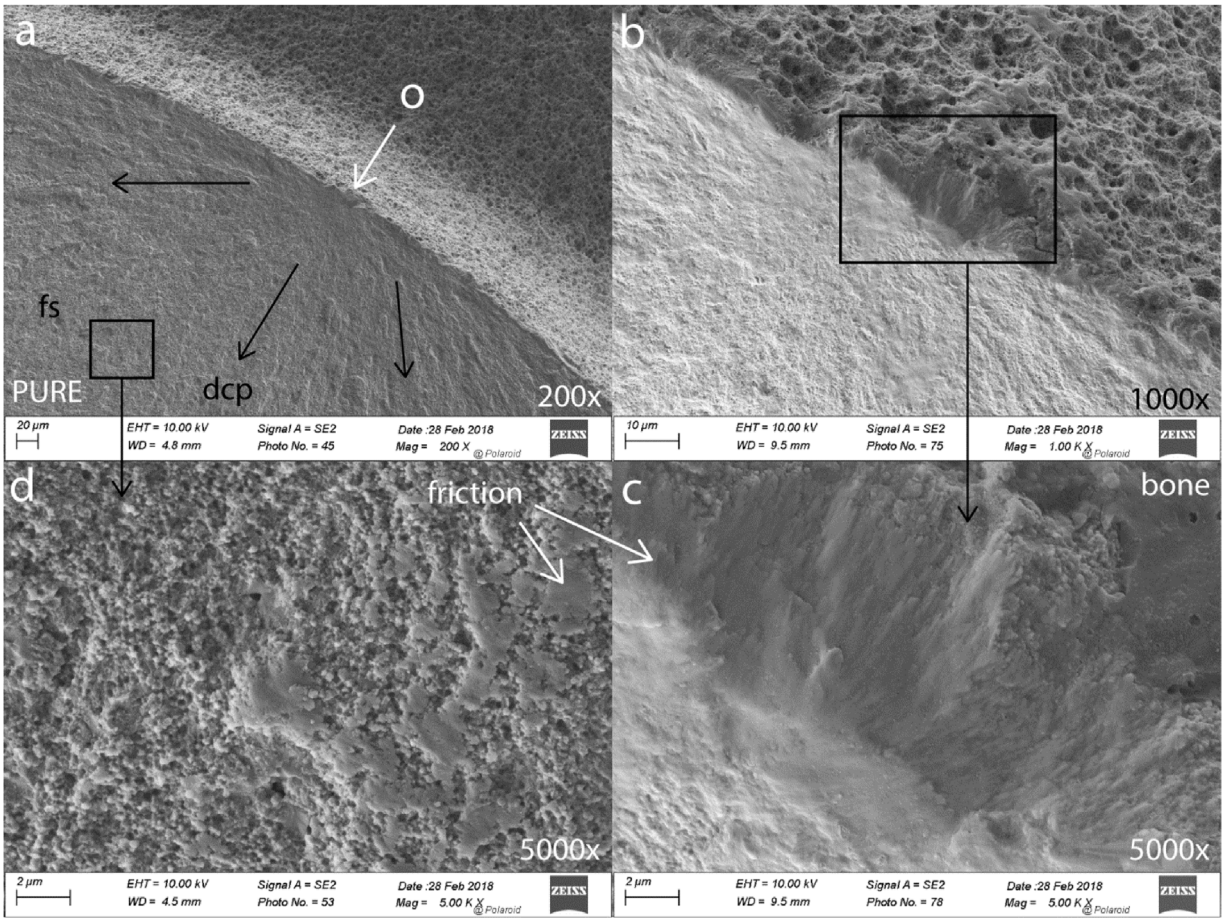

Fig. 11 – PURE Ceramic implant fracture after 18 months. On the fracture surface (fs), hackle indicate the direction of crack propagation (dcp) (Fig. 11a). The fracture origin (o) is masked by friction patterns (Fig. 11b,c), seen up to 400 μm above the origin, on the fracture surface (Fig. 11d).

as no one knows for sure which load was exercised that was responsible for fracture.

The systematic presence of a compression curl in all broken parts analyzed indicated that the implants were primarily loaded in bending or had a strong bending component [5,30]. The fractographic analysis showed that fracture originated at the periphery of the implant's inner diameter (i.e. smallest section between two threads) and adjacent to the bone level as already noticed on the X-rays. This was consistent with fracture reports in previous research papers [25,27,28,31].The implants' diameters at the constriction zone where fracture occurred were rather small and were 3.3 mm for AXIS (outer diameter of 4.1 mm), 3.7 mm for SDS (implant outer diameter of 5.0 mm), 2.7 mm for Z-Look 3 (outer diameter of 3.25 mm) and 2.7 mm for PURE Ceramic implant (outer diameter of 3.3 mm). As already demonstrated some 15 years ago, implant's diameter is more critical than implant's length [31,32]. With increasing diameter, the magnitude of stress around the implant's neck region decreases. FEM research showed that above 3.6 mm diameter the maximum stress area around the implant's neck at the bone level decreases [31]. With a poor survival of 59.6% at 3 years for Z-Look 3 narrow diameter implants [28] the Z-Systems manufacturer discontinued their production and replaced them with a modified design and increased outer diameter (3.6 mm). Indications to use were also limited to single restorations for lateral incisors and central mandibular incisors.

All failed implants had identical key fractographic features such as hackle, twist hackle and compression curl confirming a bending component in the fracture process. Measurements of critical crack sizes however were challenging in comparison to in vitro bend bars flexure tests under controlled conditions. Estimates of critical crack sizes for AXIS and SDS were around 40 μm representing stress values in the order of 600 MPa similar to in vitro fatigue testing of 3Y-TZP bend bars with machined surfaces [33]. AXIS implants had a proprietary porous coating which was definitely detrimental to the survival of the implants. AXIS implants have been hot isostatically pressed as a final processing step, but large cracks as those existing in the porous coating cannot be closed with such a process [34]. *In vitro* testing of these coated implants [35] resulted in 18% strength reduction compared to the original non-coated injection molded version. After accelerated aging of 100 h the reduction in strength was reaching 43% [35]. The transformation volume fraction of respectively 88 and 87% were found for the same coated and uncoated injec-

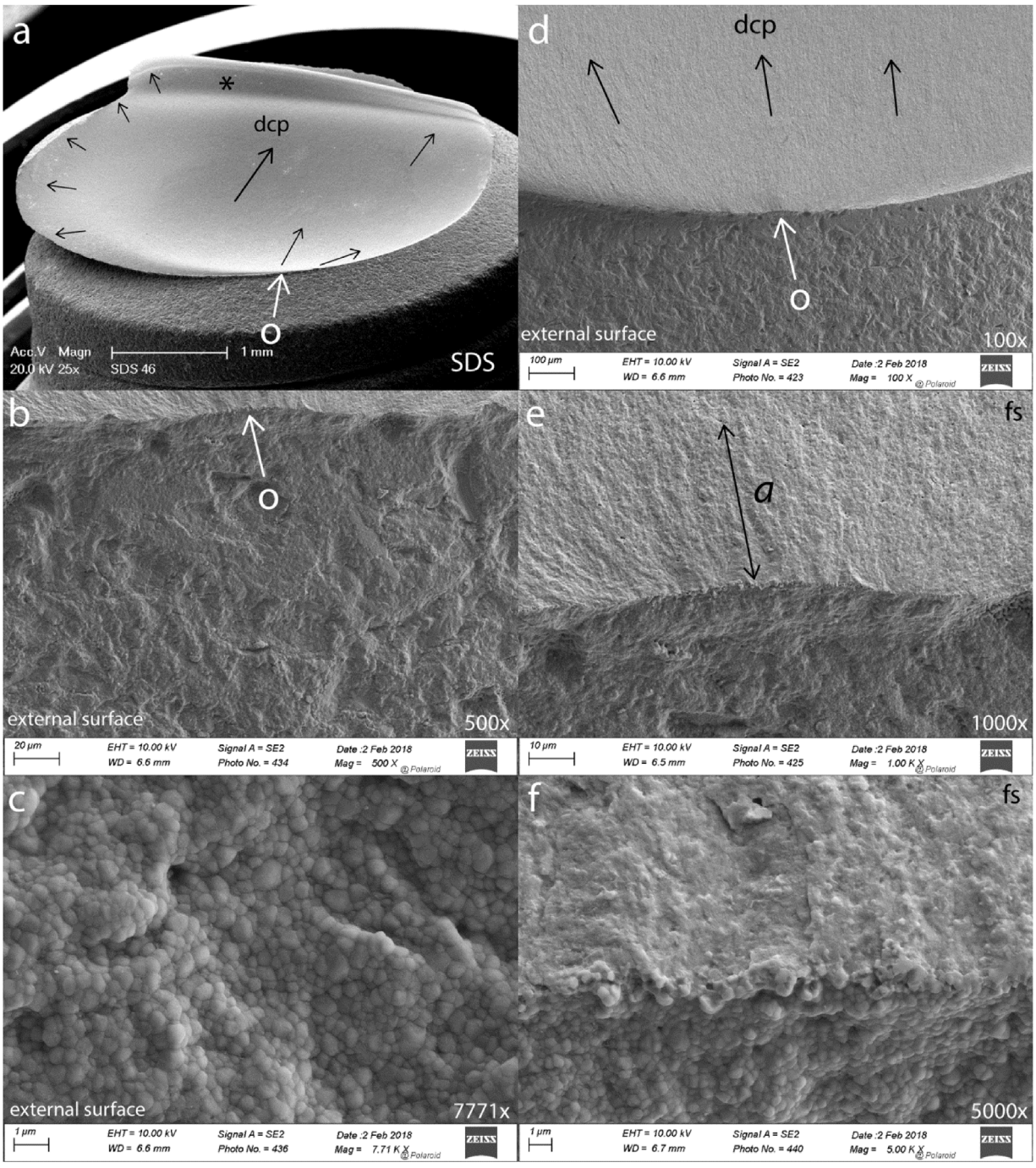

Fig. 12 – SDS 46–1 m wide diameter implant fracture after 1 months. The implant's outer surface is rough (Fig. 12a,b,d). Fracture origin (O, white arrow), direction of crack propagation (dcp) (black arrows), compression curl (*), fracture surface (fs). The critical crack depth (*a*) is approx. 36 μm (Fig. 12e). Fig. 12f is a higher magnification of Fig. 12e showing the fracture surface at the very beginning of the crack initiation. The implant's outer surface is micro-rough with fine free-air sintered grains (Fig. 12c).

tion molded zirconia with a depth of monoclinic transformed layer of respectively 13 and 14 μm showing twinning and small cracking at grain boundaries [36]. Whether aging has played a role in the fracture of the clinically failed zirconia implants in this research still has to be investigated with FIB-SEM analysis.

The fractures of the first generation of Z-Look 3 reduced implants have found a favorable terrain to develop under cyclic masticatory loadings. The combination of a very small implant diameter at fracture (~2.7 mm) together with a large grit alumina sandblasting surface treatment was detrimental to the survival of such implant. The fracture origins were clearly connected to the indent-type of dam-

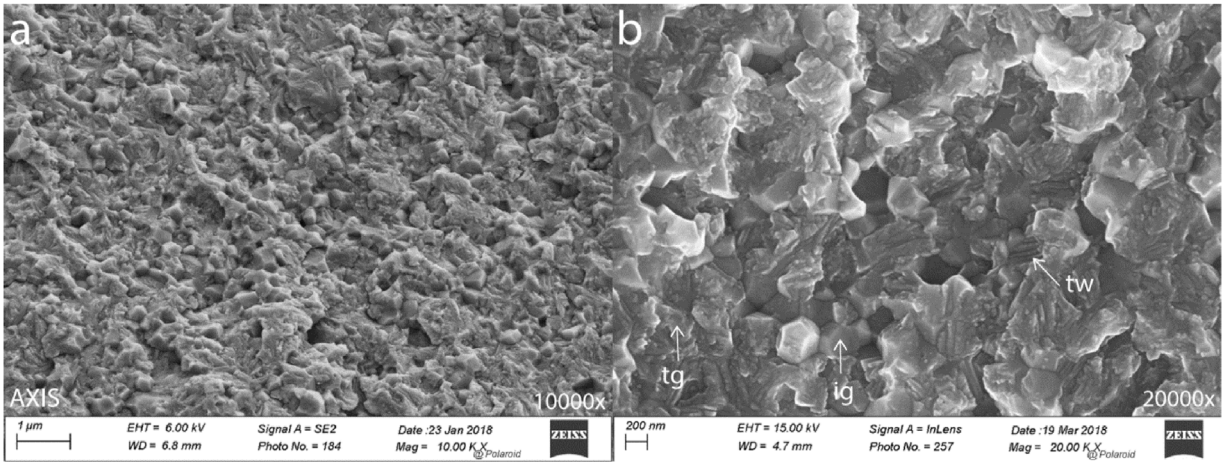

Fig. 13 – AXIS fracture surface. The microstructure shows transgranular (tg), intergranular (ig) fracture as well as twinning (tw) of the transformed zirconia grains visible by the step-like pattern.

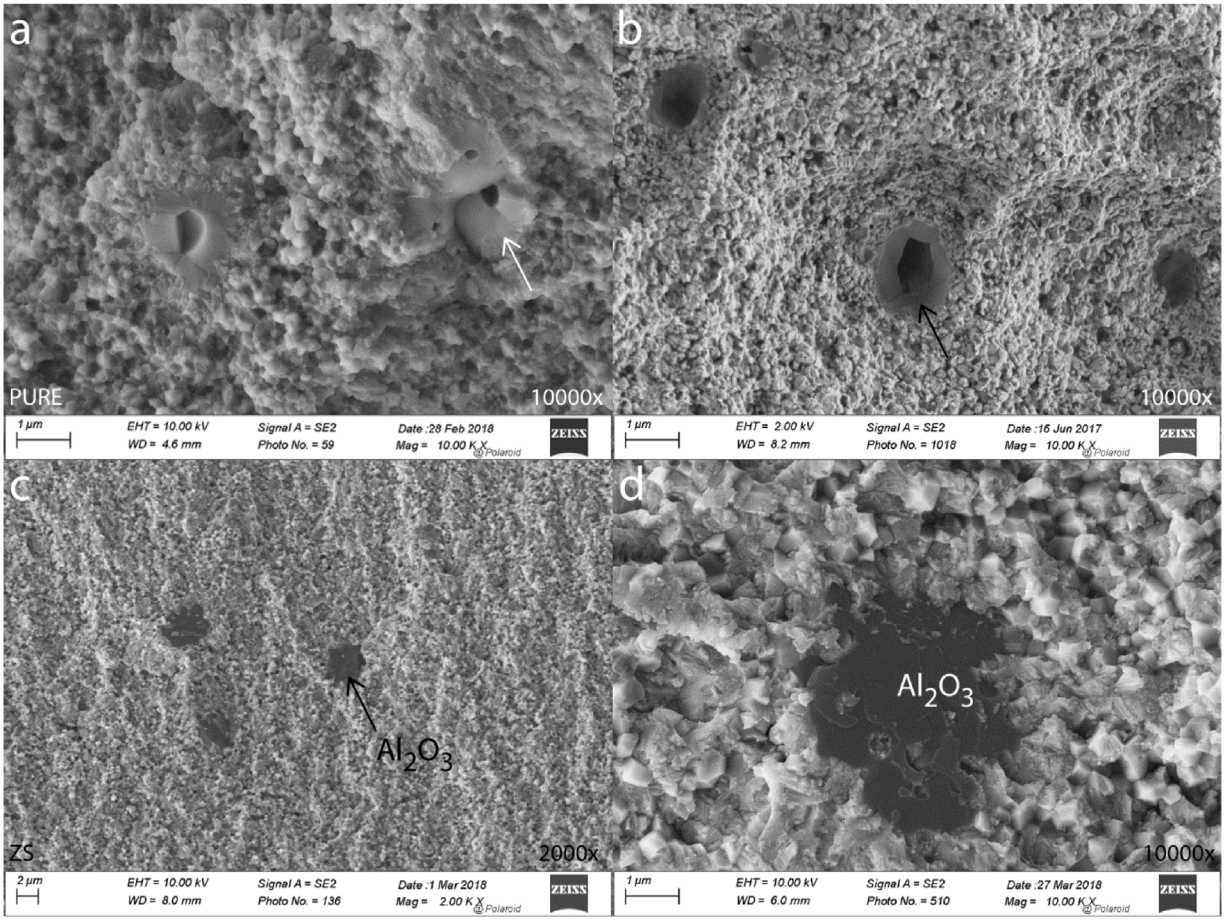

Fig. 14 – PURE Ceramic implant (a,b) and ZS 11-9y (c,d). Excessive grain growth (arrows) is seen both on the PURE Ceramic implant fracture surface (a) as well as on the implant's external acid-etched surface (b). For the Z-System implants, large (2–4 μm) Al_2O_3 particles were present on the fracture surface as shown in Fig. 14c,d.

age from large alumina particle sandblasting. Such surface treatment on 3Y-TZP tested under cyclic loading has shown to degrade the material's long-term performance [37,38]. Although alumina sandblasting may induce some favorable strengthening monoclinic phase transformation, the reliability of the zirconia is lowered [39,40]. Such aggressive sandblasting treatment (>100 μm alumina particles @ 4 bars) creates deep v-notch type defects which may act as starter

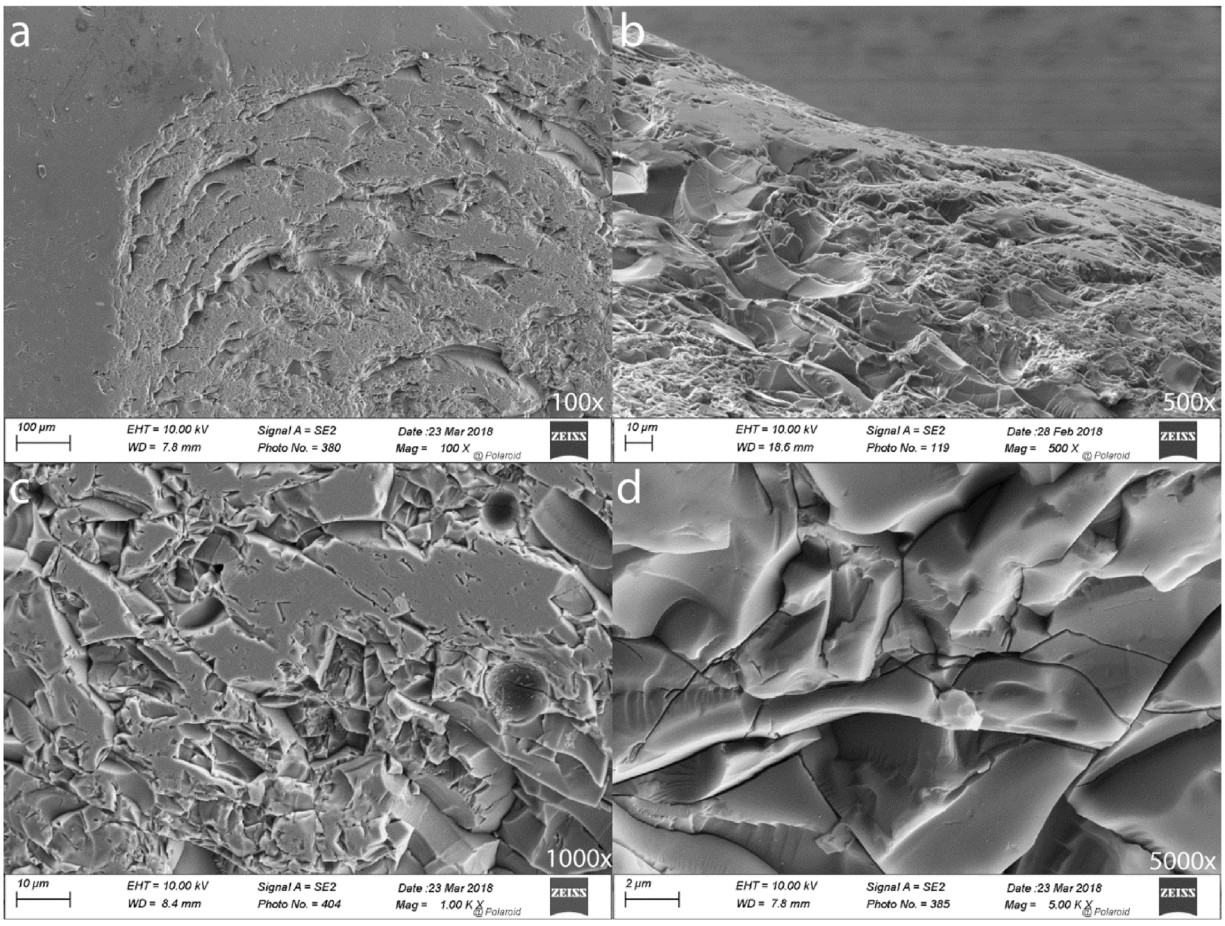

Fig. 15 – (a) Illustration of a mesio-buccal occlusal surface wear after 8 years of the ceramic crown cemented over an AXIS molar implant (AXIS 26-8y). (b) localized incisal edge wear of the lithium disilicate ceramic crown after 18 months cemented over a PURE Ceramic implant (PURE 22–18 m). The wear facet in Fig. 15a, is the result of lateral (*i.e.* buccal) excursions as seen by the concave fractured areas (sliding direction from bottom to top). Higher magnifications of Fig. 15a are shown in Fig. 15c,d with typical brittle fracture behavior showing extensive microcracking of the ceramic surface subjected to contact loading and wear.

cracks in stress concentration areas and should therefore be avoided.

The highly unusual site of fracture at mid-way inside the bone for an osseointegrated reduced diameter PURE Ceramic implant after 18 months of intraoral loading is not clear. The roughened surface obtained from sandblasting and acid-etching by the manufacturer did not seem to have created a particular critical flaw, but the site of origin was unfortunately masked by friction patterns. The patient did not comment on a special trauma event but was aware to be a bruxer as evidenced by marked wear patterns on the incisal edge of the crown. With one case only it is difficult to make any conclusions. However, considering the high level of bending and the small implant diameter at fracture (2.7 mm) the recommendation would be to exclude such high risk patients for reconstructions on small diameter zirconia implants as already strongly expressed in several papers [25,27,28]. The origin in the SDS implant was not related to any damage on the outer implant surface from the processing. The very smooth fracture surface appearance contained many very fine hackle running from distal to mesial. With no other fracture case to compare, the only explanation for such premature failure may come from high occlusal contact loading as evidenced by the important occlusal wear already seen after only one month of service. The generated bending moment and the rather small diameter at fracture (3.7 mm) for this large size crown have contributed to this early failure. It is to emphasize that this SDS 1.0 implant was from a first generation of 3Y-TZP which was discontinued in 2013. The manufacturer has since then innovated with a different zirconia implant design and surface treatment.

The microstructure seen on the fracture surfaces was similar for all implants regardless of the ceramic processing and manufacturer with a mix of intergranular and transgranular fracture. Fracture propagated predominantly transgranularly near the origin. The presence of 0.25 wt% of alumina in a 3Y-TZP composition does favor transgranular fracture [41] possibly due to an increase in the grain-boundary cohesion.

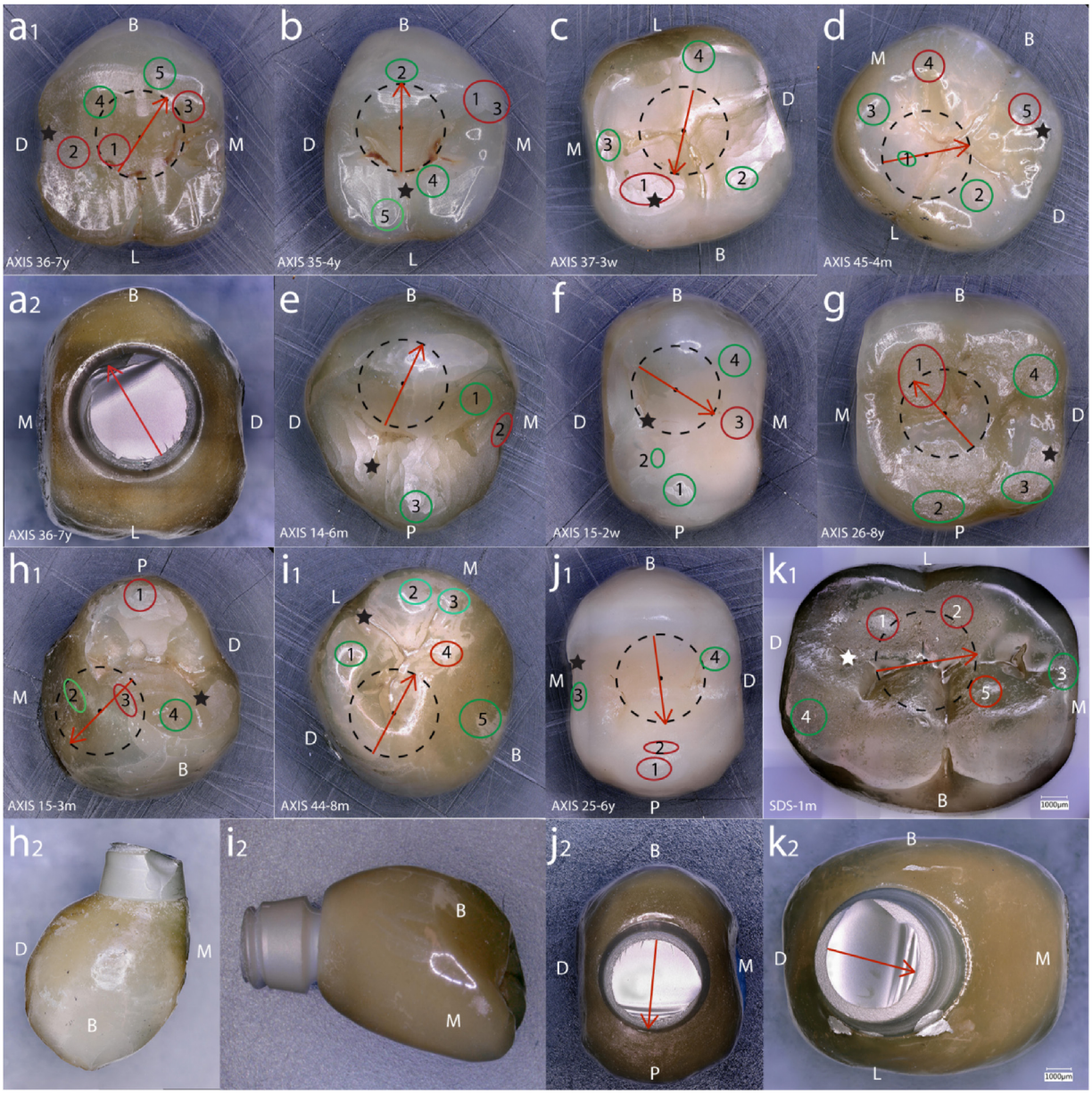

Fig. 16 – The implant center (black dot) and diameter at fracture is drawn with a dashed-line circle. The selected occlusal contacts (circles) for load distribution are numbered. Red circles represent main loading contacts (see Table 2 for load distribution). The star (*) indicates the arbitrarily chosen reference. The red arrow indicates the direction of crack propagation. The fracture origin is the starting point of the red arrow as determined from the fracture surface analyses. Fig 16a1-2: AXIS 36-7y with corresponding fracture surface view and crown orientation (B = buccal, D = distal, M = mesial, P = palatal, L = lingual); Fig. 16b: AXIS 35-4y; Fig. 16c: AXIS 37-3w; Fig. 16d: AXIS 45-4m; Fig. 16e: Axis 14-6m; Fig. 16f: AXIS 15-2w; Fig. 16g: AXIS 26-8y; Fig. 16h1–2: AXIS 15-3m, shows a that a mesial portion of the ceramic crown broke off. The front view (h2) illustrates the distal bulk extension of the crown making the central axis of the implant off-centered. Fig. 16i1–2: AXIS 44–8 m shows an off-centered implant with respect to the crown's orientation and a poorly fitted seating of the crown on the implants shoulder (i2). Fig. 16j1-2: AXIS 25-6y; Fig. 16k1-2: SDS-1m. Color image is available in the online version.

Twinning in grains seen at very high magnification, recognizable by the step-like grain surface does occur during a martensitic phase transformation from *t* to *m* or as a result of ferroelastic domain switching under the application of a stress and represent a toughening mechanisms for tetragonal metastable zirconia [10,42,43]. Larger zirconia grains, possibly cubic, seen in two implant systems (PURE Ceramic implant and Z-Systems), although not related to the fracture origin, are heterogeneities related to the processing method [44]. Large grains may be primarily cubic lowering the amount of tetragonal phase available for transformation toughening under the action of a localized stress [1,16].

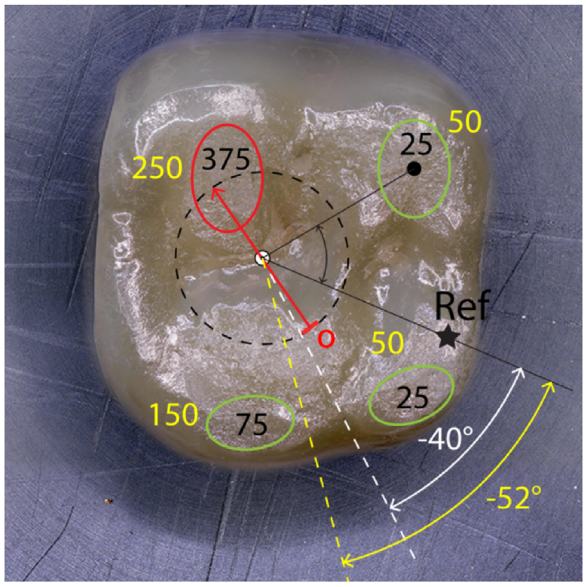

Fig. 17 – Example of how changing loads in each occlusal contact would affect the calculated angular position of the crack initiation projected onto the implant. An angle of −40° (white arrow) is shown for loads distributed as 375 N, 75 N, 25 N, 25 N matching closely the true fracture origin O. Modifying the occlusal loads to 250 N, 150 N, 50 N, 50 N would increase the angle to −52° (yellow arrow) moving away from the true fracture origin. (For interpretation of the references to colour in this figure legend, the reader is referred to the web version of this article.)

5. Conclusion

This research was performed on first generations of 3Y-TZP zirconia implants for which three out of four manufacturers have discontinued their fabrication and replaced them with newer generations of zirconia implants. Nevertheless, the failure analysis approach described in this paper combining clinical evidence with engineering science can be applied to any zirconia implant fracture in the future. The novel approach presented here was the combination of fractography and the use of a mathematical model taking into account the crown-implant's spatial coordinates and occlusal contacts, generating information on bending moment, resultant stress and location of the crack onset on the implant. Special attention should be given to occlusal contacts on the crown showing pronounced wear with respect to the implant's center as off-axis loading increases bending. For clinical trials, it is important not only to mention a survival rate but to describe if the failure was biological or of mechanical origin. In case of fracture, researchers are encouraged to go through the needed full failure analysis as described in this paper. Every single fracture will have its amount of tale-telling information, whether it is related to material processing, implant design or critical bending from occlusal loading. One has to remember, that the surgical procedure related to the retrieval of a broken implant which is fully osseointegrated is quite traumatic for the patient, often involves bone grafting, additional healing times, discomfort and additional costs. With current available digital planning, correct implant placing and final crown reconstruction can be ideally designed limiting off-centered contacts with respect to the implant's central axis.

Acknowledgments

The authors would like to thank Dr. Isabelle L. Denry and Dr. Paulo F. Cesar for their expert opinion and fruitful discussions.

Appendix A.

Axis Z Axis of the implant towards the occlusal crown surface

Axis X Arbitrary reference identified on the occlusal crown surface

Axis Y Complement of Z and X

O Intersection of Z with the fracture surface

O,X,Z: P Plane of reference

O,X,Y,Z Reference

Ci Center of the occlusal contact surface #i

O,Xi,Z Pi: plane through the implant axis and Ci

Ci,Xi,Yi,Z Reference through surface contact #i

θi Angle between P and Pi

OCi ri Xi + zi Z

ni Vector normal to the occlusal crown surface in Ci

αi Angle between Z and the projection of ni on Pi

βi Angle between Z and the projection of ni on Ci,Yi,Z

xi ri × COS(θi)

yi ri × SIN(θi)

ai TAN(αi)

bi TAN(βi)

φi ATAN(βi/αi)

ψi ROOT(αi × αi + βi × βi)

Ni Force following the normal to the contact, >0 if directed towards the contact

Ti Force following the contour line (most often negligible)

Li Force following the line of greatest slope, >0 if directed from the top of a cusp outwards

Force in Xi, Yi, Zi

FXi	Ni × SIN(ψi) × COS(θi + φi)-Ti × SIN(θi + φi) + Li × COS(ψi) × COS(θi + φi)
FYi	−Ni × SIN(ψi) × SIN(θi + φi) + Ti × COS(θi + φi) + Li × COS(ψi) × SIN((θi + φi)
FZi	−Ni × COS(ψi)-Li × SIN(ψi)

Moment of force on the fracture surface

MAXi	yi × FZi-zi × FYi
MAYi	zi × FXi-xi × Fzi
MAZi	xi × FYi-yi × FXi
RBX	Resultant Bending/X: SUM of MAXis
RBY	Resultant Bending/Y: SUM of MAYis
RT	Resultant Torsion: SUM of MAZis
RB	Resultant Bending: ROOT(RBX × RBX + RBY × RBY)

Shear stress (τ) (RT × 16/3.14/w³)

Tensile stress (σ) (RB × 32/3.14/w³)

Max principal stress (σ_{max}) $1/2(\sigma + ROOT(\sigma^2 + 4\tau^2))$

von Mises equivalent (vM) $ROOT(\sigma \times \sigma + 3 \times \tau \times \tau)$

angular position of crack origin from arbitrary Ref (>0 = counterclock) ATAN(RBY/RBX)

REFERENCES

[1] Denry I. How and when does fabrication damage adversely affect the clinical performance of ceramic restorations. Dent Mater 2013;29:85–96.
[2] ASTM-C1322-15. Standard Practice for Fractography and Characterization of Fracture Origins in Advanced Ceramics. ASTM International; 2015.
[3] Quinn JB, Quinn GD, Kelly JR, Scherrer SS. Fractographic analyses of three ceramic whole crown restoration failures. Dent Mater 2005;21:920–9.
[4] Belli R, Scherrer SS, Lohbauer U. Report on fractures of trilayered all-ceramic fixed dental prostheses. Case Stud Eng Fail Anal 2016;7:71–9.
[5] Scherrer SS, Lohbauer U, Della Bona A, Vichi A, Tholey MJ, Kelly JR, et al. ADM guidance-Ceramics: guidance to the use of fractography in failure analysis of brittle materials. Dent Mater 2017;33:599–620.
[6] Lohbauer U, Amberger G, Quinn GD, Scherrer SS. Fractographic analysis of a dental zirconia framework: a case study on design issues. J Mech Behav Biomed Mater 2010;3:623–9.
[7] Scherrer SS, Quinn GD, Quinn JB. Fractographic failure analysis of a Procera AllCeram crown using stereo and scanning electron microscopy. Dent Mater 2008;24:1107–13.
[8] Depprich R, Naujoks C, Ommerborn M, Schwarz F, Kübler NR, Handschel J. Current findings regarding zirconia implants. Clin Implant Dent Relat Res 2014;16:124–37.
[9] Chevalier J. What future for zirconia as a biomaterial. Biomaterials 2006;27:535–43.
[10] Deville S, Chevalier J, El Attaoui H. Atomic force microscopy study and qualitative analysis of martensite relief in zirconia. J Am Ceram Soc 2005;88:1261–7.
[11] Kelly JR, Denry I. Stabilized zirconia as a structural ceramic: an overview. Dent Mater 2008;24:289–98.
[12] Piconi C, Maccauro G. Zirconia as a ceramic biomaterial. Biomaterials 1999;20:1–25.
[13] Chevalier J, Gremillard L, Deville S. Low-temperature degradation of Zirconia and implications for biomedical implants. Annu Rev Mater Res 2007;37:1–32.
[14] Wei C, Gremillard L. Towards the prediction of hydrothermal ageing of 3Y-TZP bioceramics from processing parameters. Acta Mater 2018;144:245–56.
[15] Wei C, Gremillard L. The influence of stresses on ageing kinetics of 3Y-and 4Y-stabilized zirconia. J Eur Ceram Soc 2018;38:753–60.
[16] Chevalier J, Gremillard L, Virkar AV, Clarke DR. The Tetragonal-Monoclinic Transformation in Zirconia: Lessons Learned and Future Trends. J Am Ceram Soc 2009;92:1901–20.
[17] Jimenez-Pique E, Ramos A, Munoz-Tabares JA, Hatton A, Soldera F, Mucklich F, et al. Focused ion beam tomography of zirconia degraded under hydrothermal conditions. J Eur Ceram Soc 2012;32:2129–36.
[18] Thoma DS, Ioannidis A, Cathomen E, Hämmerle CHF, Hüsler J, Jung RE. Discoloration of the peri-implant mucosa caused by zirconia and titanium implants. Int J Periodontics Restorative Res 2016;36:39–45.
[19] Sivaraman K, Chopra A, Narayan AI, Balakrishnan D. Is zirconia a viable alternative to titanium for oral implant? A critical review. J Prosthodont Res 2018;62:121–33.
[20] Hashim D, Cionca N, Courvoisier DS, Mombelli A. A systematic review of the clinical survival of zirconia implants. Clin Oral Investig 2016;20:1403–17.
[21] Cionca N, Hashim D, Mombelli A. Zirconia dental implants: where are we now, and where are we heading? Periodontology 2017 2017;73:241–58.
[22] Osman RB, Swain MV. A critical review of dental implant materials with an emphasis on Titanium versus Zirconia. Materials 2015;8:932–58.
[23] Pieralli S, Kohal RJ, Jung RE, Vach K, Spies BC. Clinical outcomes of Zirconia dental implants: a systematic review. J Dent Res 2017;96:38–46.
[24] Siddiqi A, Khan AS, Zafar S. Thirty years of translational research in Zirconia dental implants: a systematic review of the literature. J Oral Implantol 2017;43:314–26.
[25] Gahlert M, Burtscher D, Grunert I, Kniha H, Steinhauser E. Failure analysis of fractured dental zirconia implants. Clin Oral Implants Res 2012;23:287–93.
[26] Osman RB, Ma SY, Duncan W, De Silva RK, Siddiqi A, Swain MV. Fractured zirconia implants and related implant designs: scanning electron microscopy analysis. Clin Oral Implants Res 2013;24:592–7.
[27] Roehling S, Woelfler H, Hicklin S, Kniha H, Gahlert M. A retrospective clinical study with regard to survival and success rates of Zirconia implants up to and after 7 years of loading. Clin Implant Dent Relat Res 2016;18: 545–58.
[28] Gahlert M, Burtscher D, Pfundstein G, Grunert I, Kniha H, Roehling S. Dental Zirconia implants up to three years in function: a retrospective clinical study and evaluation of prosthetic restorations and failures. Int J Oral Maxillofac Implants 2013;28:896–904.
[29] Al-Omiri MK, Sghaireen MG, Alhijawi MM, Alzoubi IA, Lynch CD, Lynch E. Maximum bite force following unilateral implant-supported prosthetic treatment: within-subject comparison to opposite dentate side. J Oral Rehabil 2014;41:624–9.
[30] Quinn GD. A NIST recommended practice guide: Fractography of Ceramics and Glasses. Special Publication 960-16e2. Washington, DC: National Institute of Standards and Technology; 2016 http://nvlpubs.nist.gov/nistpubs/specialpublications/NIST.SP.960-16e2. pdf.
[31] Himmlova L, Dostalova T, Kacovsky A, Konvickova S. Influence of implant length and diameter on stress distribution: a finite element analysis. J Prosthet Dent 2004;91: 20–5.
[32] Holmgren EP, Seckinger RJ, Kilgren LM, Mante F. Evaluating parameters of osseointegrated dental implants using finite element analysis–a two-dimensional comparative study examining the effects of implant diameter, implant shape, and load direction. J Oral Implantol 1998;24:80–8.
[33] Scherrer SS, Cattani-Lorente M, Vittecoq E, de Mestral F, Griggs JA, Wiskott HW. Fatigue behavior in water of Y-TZP zirconia ceramics after abrasion with 30 mum silica-coated alumina particles. Dent Mater 2011;27:e28–42.
[34] Scherrer SS, Cattani-Lorente M, Yoon S, Karvonen L, Pokrant S, Rothbrust F, et al. Post-hot isostatic pressing: a healing treatment for process related defects and laboratory grinding damage of dental zirconia. Dent Mater 2013;29:e180–90.
[35] Sanon C, Chevalier J, Douillard T, Cattani-Lorente M, Scherrer SS, Gremillard L. A new testing protocol for zirconia dental implants. Dent Mater 2015;31:15–25.
[36] Cattani-Lorente M, Scherrer SS, Durual S, Sanon C, Douillard T, Gremillard L, et al. Effect of different surface treatments on the hydrothermal degradation of a 3Y-TZP ceramic for dental implants. Dent Mater 2014;30:1136–46.
[37] Zhang Y, Lawn BR. Fatigue sensitivity of Y-TZP to microscale sharp-contact flaws. J Biomed Mater Res B Appl Biomater 2005;72:388–92.

[38] Zhang Y, Lawn BR, Rekow ED, Thompson VP. Effect of sandblasting on the long-term performance of dental ceramics. J Biomed Mater Res B 2004;71b:381–6.
[39] Kosmac T, Oblak C, Jevnikar P, Funduk N, Marion L. The effect of surface grinding and sandblasting on flexural strength and reliability of Y-TZP zirconia ceramic. Dent Mater 1999;15:426–33.
[40] Kosmac T, Oblak C, Jevnikar P, Funduk N, Marion L. Strength and reliability of surface treated Y-TZP dental ceramics. J Biomed Mater Res 2000;53:304–13.
[41] Samodurova A, Kocjan A, Swain MV, Kosmac T. The combined effect of alumina and silica co-doping on the ageing resistance of 3Y-TZP bioceramics. Acta Biomater 2015;11:477–87.
[42] Chien FR, Ubic FJ, Prakash V, Heuer AH. Stress-induced martensitic transformation and ferroelastic deformation adjacent microhardness indents in tetragonal zirconia single crystals. Acta Mater 1998;46:2151–71.
[43] Virkar AV, Matsumoto RLK. Ferroelastic domain switching as a toughening mechanism in tetragonal Zirconia. J Am Ceram Soc 1986;69:C224–6.
[44] Denry I, Kelly JR. State of the art of zirconia for dental applications. Dent Mater 2008;24:299–307.